Chapter 1   Introduction

1.1 Introduction of photonic crystals

Photonic crystal is a novel technology to confine or forbid different wavelength of light or in the certain material arranged periodically, this concept was first produced by Eli Yablonovitch and S.John. [1-2]. At first Yablonovitch wanted to improve the spontaneous emission loss form laser, he thought using photonic band gap around atoms and decrease the loss of spontaneous emission from atoms. Then "photonic crystal" was present to mankind soon and the research of it became more importantly. Now research of photonic crystal grow quickly and close to our life, among these years, photonic crystal research can separate into several main parts, like photonic crystal laser; photonic crystal waveguide and photonic crystal fiber …etc.

Simply speaking, there are three types of photonic crystals, one-dimensional photonic crystal, two-dimensional photonic crystal, three-dimensional photonic crystal.(fig. 1.1)[3]
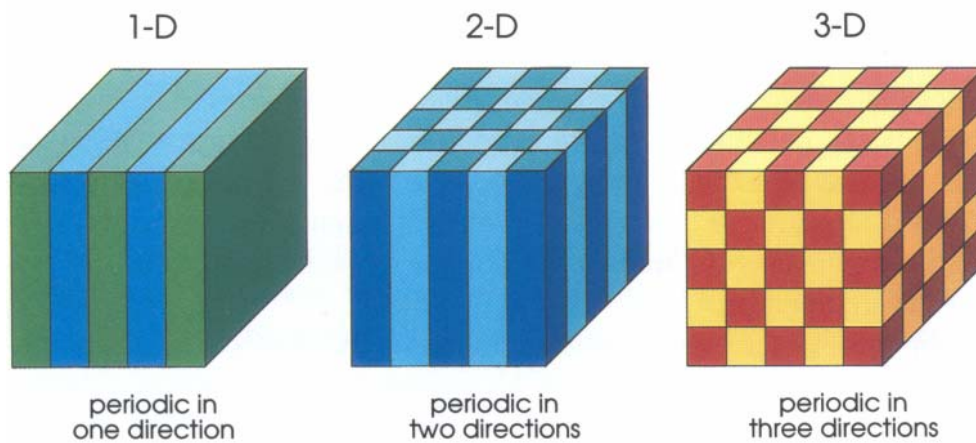

Fig. 1.1 Simple examples of one-dimensional, two-dimensional, three-dimensional photonic crystals and different colors represent different dielectric constant of material. [2]

First, one-dimension photonic crystal is like Distributed Bragg Reflector (DBR) using different materials stack up layer by layer, then it can enhance transmission of reflection of certain band of light wavelength, it is used extensively in human day life ,for example,

multi-films of glasses, it can enhance the transmission of visible light and reflection of ultraviolet to protect eyes of people, reflection mirror of lasers…etc.

Second, dielectric constants of materials change periodically in two-dimension is call "two-dimensional photonic crystal", generally speaking, 2-D photonic crystal arrangement can simply divide into two kinds. One is square-lattice, another is triangular-lattice, the different arrangement of photonic crystal would effect the forbidden bad for TE wave or TM wave. In two-dimensional photonic crystal, the polarization of light is important, in 2-D situation, TE(TM) wave indicate that electric (magnetic) field is in in-plan direction which dielectric constants change periodically, and magnetic (electric) field is in vertical direction which dielectric constants don't change along this direction (fig. 1.2). For example, 2-D triangular air holes photonic crystal, the band-gap (fig. 1.3 (a)) is forbidden for TE wave, but not for TM. The band-gap (fig. 1.3 (b)) of 2-D square dielectric rods photonic crystal is contrary to triangular air holes, band-gap is forbidden for TM wave, not TE wave. In Photonic crystal, one air hole or a row of air holes can be removed to form a defect mode in photonic crystal. Then depending on our design, let light propagate in photonic crystal and reduce in-plane loss by photonic crystal band-gap effect can be achieved.
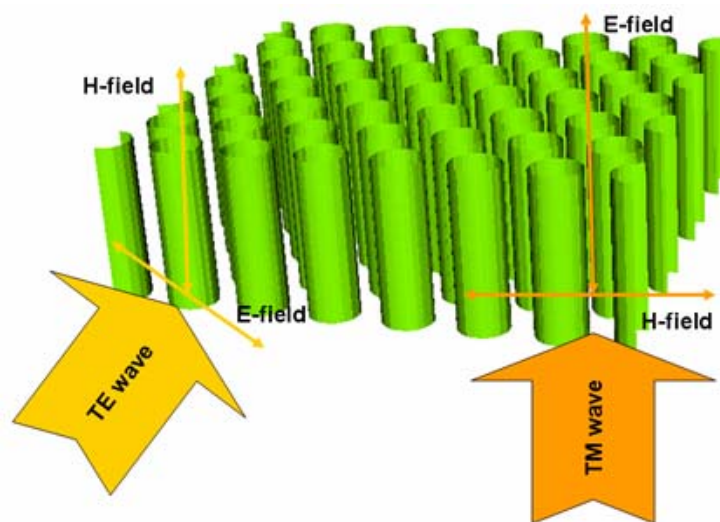

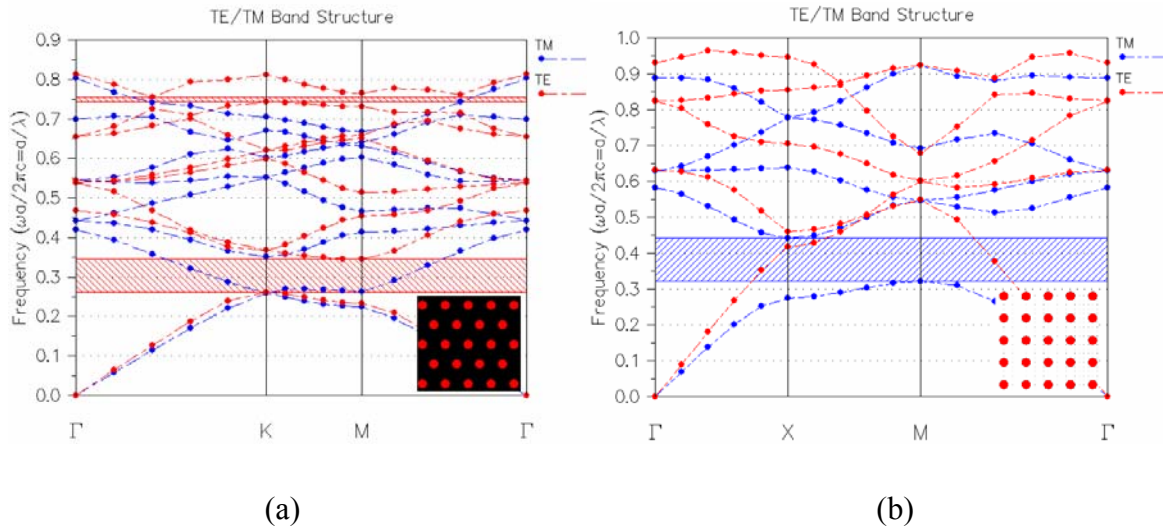Fig. 1.2 E-field and H-field for TE and TM wave in two-dimensional photonic crystal structure

<center>(a)   (b)</center>

Fig. 1.3 (a)Bad-gap of 2D air holes triangular photonic crystal. (b) Bad-gap of 2-D dielectric rods photonic crystal.

Third, three-dimensional photonic crystal structure is more complex than one-dimensional and two-dimensional photonic crystal, not only simulation but also fabrication. But the result of three-dimensional photonic crystal is more better than two-dimensional photonic crystal, it has full TE and TM band-gap where no light can propagation through it (fig. 1.4) . for example, diamond structure was also called Yablonovite, it had complete band-gap for TE and TM wave which was first found by Yablonovitch [4].
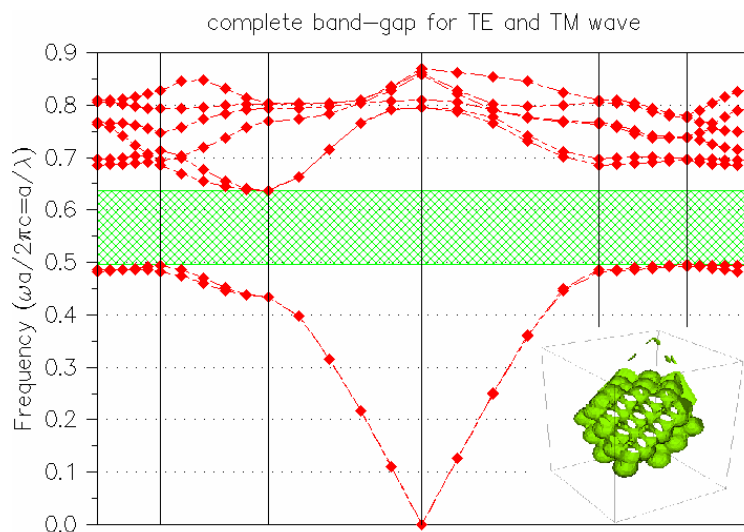

Fig. 1.4 The complete band-gap of three-dimensional diamond structure photonic crystal

<center>3</center>

1.2 Applications of photonic crystals

So far, the research topics of photonic crystal are very much, the main topics are photonic crystal lasers、photonic crystal waveguides、photonic crystal fiber...etc. Although the applications are diversified, the final target is to utilize those properties of photonic crystal to realize photonic integrated circuits.

1.2.1 Photonic crystal lasers

In the part of photonic crystal lasers, generally dividing into two types, the cavity of laser and band-edge laser. The cavity of laser was first proposed in 1994 [5] and demonstrated in 1999 by O. Painter et al [6]. The cavity of laser use photonic band-gap to confine light in the lateral direction, but vertical confinement use the index difference of active region and air. The typical photonic crystal cavity of laser structure is show in fig. 1.5 [6]. The benefits of photonic crystal cavity of laser are low threshold current, small mode volume, and high quality factor, it has more advantages than conventional semiconductor laser. Band-edge laser utilizes the band-edge characteristics of photonic crystal band-gap. At the band-edge region, the slope of band-gap almost became to zero, the velocity of photon in photonic crystal tended toward zero, it is also called "slow light". Because the velocity of light becomes slow then the reaction time between radiate material would increase, finally spontaneous emission can be enhanced by band-edge effect. The disadvantages of band-edge laser are more high threshold current and low quality factor than the cavity of laser, but the high output power(>20mw) and low dispersion angle are better than the cavity of laser.
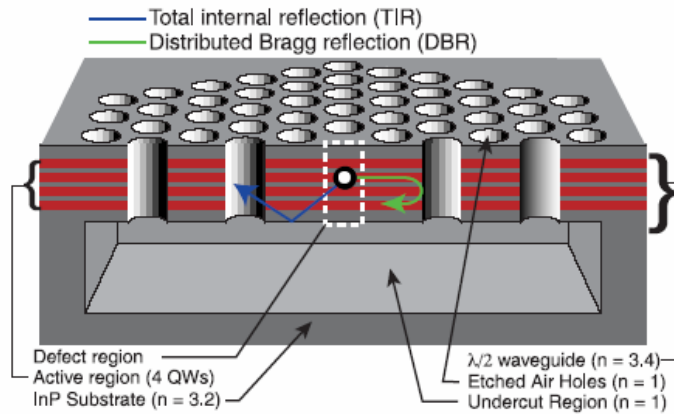
Fig. 1.5 The typical photonic crystal cavity of laser structure. [6]

1.2.2 Photonic crystal fibers

Photonic crystal fiber is constructed by the unique cladding structure of this kind of fibers, conventional fiber propagate light by total internal reflection between the core with high index embedded in a cladding with low index. The index difference in photonic crystal fiber is obtained by periodical variation in the cross section with high and low index material. For example, in fig. 1.6 (a) A standard optical fiber, formed using two bulk materials (core diameter 9µm), (b)An index-guiding photonic crystal fiber (core diameter 5µm) and (c) A hollow-core photonic band-gap fiber (core diameter 7µm) [7]. The photonic crystal band-gap effect can let light confined in the core and cant leak to air, the breakthroughs of photonic crystal are lager mode area with single mode operation and large numerical aperture.

5
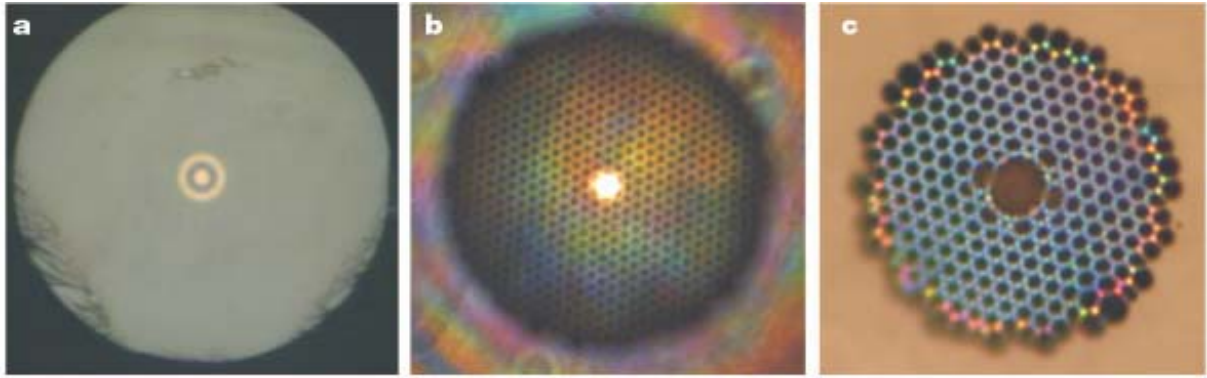
| (a) | (b) | (c) |

Fig 1.6 (a) A standard optical fiber (b) An index-guiding photonic crystal fiber (c)A hollow-core photonic band-gap fiber.

1.2.3 Photonic crystal waveguides

The line defect or point defect in photonic crystal produce a defect mode in forbidden band-gap and can be designed as power-splitter, broad-band and high transmission at sharp bend、the waveguide couple to waveguide or cavity mode in photonic crystal …etc., it will explain clearly in chapter 1.3 .
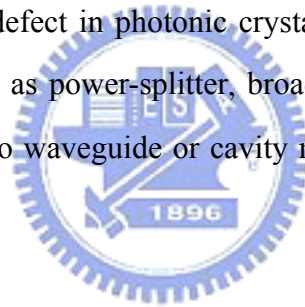
1.3 Photonic crystal waveguides (PCWG) and bends

The research of photonic crystal waveguides are more extensive, the topics of it have many development such like photonic crystal waveguide bend、coupling properties of photonic crystal waveguide、power-splitter photonic crystal ...etc. The concept of photonic crystal waveguide is utilized the defect mode in photonic crystal which some rows of air holes are removed, then some frequencies of light can propagate within the material with high index and the frequencies are in the forbidden band-gap. In the lateral direction light is restricted by photonic crystal band-gap, the wavelength is called defect mode wavelength. Line-defect waveguide was first fabricated by J.D. Joannopoulos in 1998 [8], the first device is square lattice rods and the measurement transmission of 90^0-bend region can get almost 100 percent.

The simulation result of this line-defect structure was presented in 1996[9]. In 1999 Toshiniko Baba observe light propagation in photonic crystal waveguide [10]. The year after 1999[11], Baba group bond the wafer to SiO_2 and clearly observe the propagation of light in photonic band-gap. In 2000 Hirohito Yamada fabricate the 120^0-bend photonic crystal waveguide and measure it [12]. After the basic properties of line-defect bend photonic crystal device was presented and observed, more papers to improve the transmission of 60^0-bend and 120^0-bend are studied. Most adjustments at the bend region are changing or adding some particular air holes, the research have been studied by、Susumu Noda[13-15], J.D. Joannopoulos [7-8], M. Kristensen[16]...etc[17-21]. Especially M. Kristensen group, they use topology to optimize the bend region and get over 200nm band-width of high transmission of double 60^0-bend、 90^0-bend and 120^0-bend [22-25], the device are shown in fig. 1-7(a)[22], fig. 1-7(b)[23], fig. 1-7(c)[24] and fig. 1.8 show some simple turning of air holes positions[26]. Although the result of topology optimization get high transmission and broad-band wavelength, but it has complex mathematic calculation. Trying to get the same result, the simple way to put a plane mirror at bend-region has been achieved by O. Panter group in 2004 [20], the SEM image of their device is shown in fig. 1.9. In this paper, the position adjustments of air holes at bend region do not been discussed. Putting plane mirrors at bend-region and tuning the width of mirrors are the main part of this paper, the simulation and fabrication will hardly studied in chapter 3 and chapter 4.
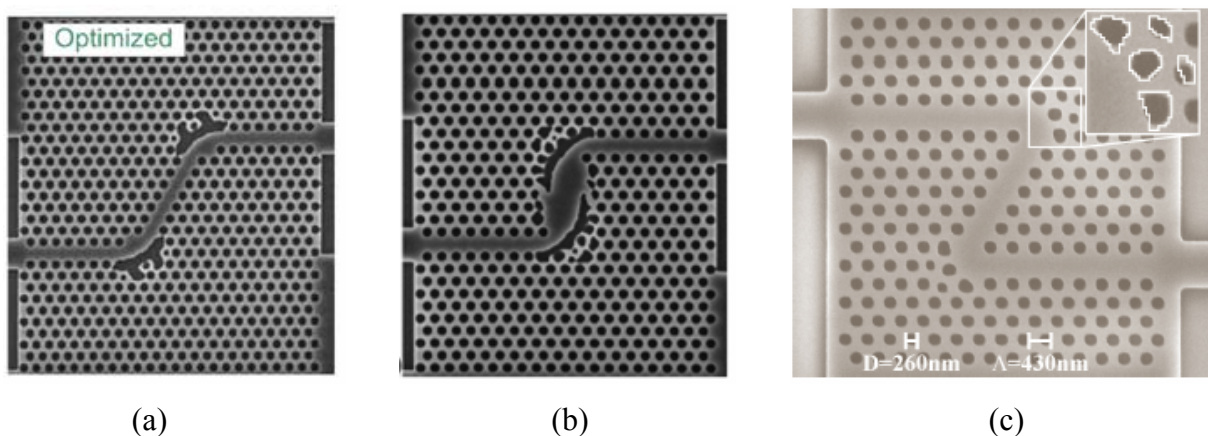

<div align="center">(a)   (b)   (c)</div>

Fig. 1.7(a), (b), (c) The SEM figures of double 60^0-bend、90^0-bend and 120^0-bend devices of topology design [22-24].
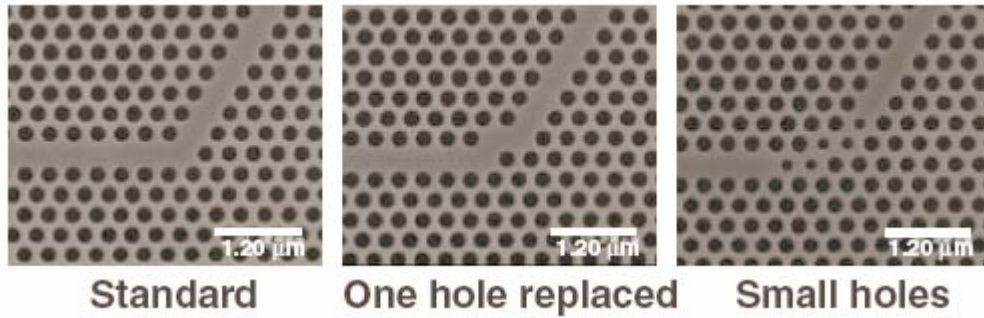
Fig. 1.8 Simple tunings of air holes positions are at bend region. [25]
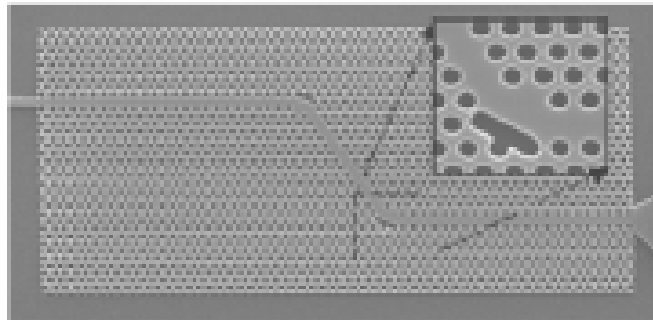

Fig. 1.9 The SEM figure of double 60^0-bend using two plane mirrors at bend region [20].

Recent years coupling properties in photonic crystal has also discussed, first coupling phenomenon is experimented by H.Yamada in 2001[27], the coupling length is 21um and around 1.5um. Then the theory was presented by Carlo. G. Someda group [28], they found the waveguide coupled to another by mode converted in the photonic crystal. The formula (1) clearly indicated that coupling length related to the difference between k value of even mode and odd mode.

$$L_B = \frac{2\pi}{|k_{y,even} - k_{y,odd}|} \quad \cdots\cdots\cdots\cdots\cdots\cdots\cdots\cdots\cdots\cdots\cdots\cdots\cdots\cdots\cdots\cdots (1)$$

Then they add air holes in the coupling region to change the band-structure and the coupling length become infinite. Easily they utilize the coupling and decoupling to get simple power-splitter for some critical wavelength. Soon more about decreasing coupling length, increasing coupling transmission have been studied. The coupling properties between

waveguide and waveguide have been discussed completely and more research to investigate cavity coupling to cavity in the waveguide since 1999 [29]. Now the CROW device has been achieve and measured in 2005 by Richard M De La Rue1 et al [30].

1.4 Conclusion

In chapter one, the basic characteristics of photonic crystal has been explained and applications of photonic crystal has been introduced. Light propagation is forbidden by the photonic crystal band-gap and the polarization of electric and magnetic wave has introduced in chapter 1-1 , the applications of photonic such as photonic crystal cavity of laser, photonic crystal fibers in chapter 1-2 and some typical photonic waveguides in 1-3,. In last chapter, we will discuss the design for bend region for high transmission and broad-band photonic crystal.

Chapter 2   Theory of calculation methods

2.1 Introduction of calculation methods

Most light propagation problems must first analyze by the four Maxwell formulas, the fundamental calculation concepts of photonic crystal is also by these formulas. In cgs unit, they are

$$\nabla \cdot B = 0$$

$$\nabla \cdot D = 4\pi\rho$$

$$\nabla \times E = -\frac{1}{c}\frac{\partial B}{\partial t}$$

$$\nabla \times H = \frac{1}{c}\frac{\partial B}{\partial t} + \frac{4\pi}{c}J \qquad \text{……………………….…… 2.1}$$

Where E and H are the macroscopic electric and magnetic fields, D and B are the displacement and magnetic induction fields, and ρ and J are the free charge and current densities. Without free charges and currents in our calculation, we set ρ and J to be zero in periodic dielectric medium.

Generally, the component D is more complex, it has a complicated power series whit electric field E, the power series is show as

$$D_i = \sum_j \varepsilon_{ij}E_j + \sum_j kx_{ijk}E_jE_k + O(E^3) \qquad \text{…………………………… 2.2}$$

For many dielectric materials, we usually assume the field strength are small enough so that we are in the linear regime, it means χ and all higher terms can be ignored. And, we also assume the material is macroscopic and isotropic, so that $E(\gamma, \omega)$ and $D(\gamma, \omega)$ are related by a scalar dielectric constant $\varepsilon(\gamma, \omega)$. Any explicit frequency dependence of the dielectric constant

are also been ignore. The last assumption is that we focus only on low-loss dielectrics, which means we treat ε(γ) as pure real. Hence, we have a brief expression as relating **D** and **E** fields.
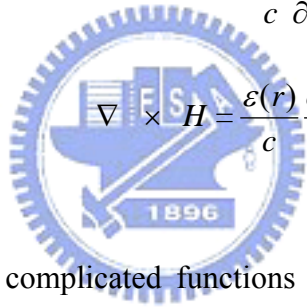
$$D(r) = \varepsilon(r)E(r)$$ …………………………………….... 2.3

Such a simplification process can also be performed in **B** and **H**. For most dielectric materials of interest, the magnetic permeability μ(r) is very close to unity and we may set **B=H**. With four assumption above, the Maxwell equations Eq. (2.1) become

$$\nabla \cdot B = 0$$

$$\nabla \cdot D = 0$$

$$\nabla \times E = -\frac{1}{c}\frac{\partial B}{\partial t}$$

$$\nabla \times H = \frac{\varepsilon(r)}{c}\frac{\partial E}{\partial t}$$ …………………............. 2.4

in general both **E** and **H** are complicated functions of time and space, and the Maxwell equations are linear. We can separate out the time dependence by expanding the fields into a set of harmonic modes. We employ the familiar trick of using a complex-valued field for mathematical convenience, and the physical fields can be obtained by taking the real part. Hence we write a harmonic mode as a certain field pattern times a complex exponential.

$$H(r,t)=H(r)e^{iwt}$$

$$E(r,t)=E(r)e^{iwt}$$ …………..…………………………….. 2.5

Because there is no free charge and current, the electromagnetic waves considered to be transverse. By eliminating Eq. (2.5) in Eq.(2.4) we can obtain the following equations;

$$\Phi_E \vec{E}(\vec{r}) \equiv \frac{1}{\varepsilon(\vec{r})} \nabla \times \{\nabla \times \vec{E}(\vec{r})\} = \frac{\omega^2}{c^2} \vec{E}(\vec{r}) \quad \ldots\ldots\ldots\ldots\ldots\ldots\ldots\ldots\ldots\text{ 2.6}$$

$$\Phi_E \vec{H}(\vec{r}) \equiv \nabla \times \{\frac{1}{\varepsilon(\vec{r})} \nabla \times \vec{H}(\vec{r})\} = \frac{\omega^2}{c^2} \vec{H}(\vec{r}) \ldots\ldots\ldots\ldots\ldots\ldots\ldots\ldots\text{ 2.7}$$

Solving Eqs. (2.6) and (2.7) are the eigenvalue problems, and we can easily prove that Φ_H is a special type of linear operator known as a Hermitian operator. The eigenvectors *H(r)* and

$\tilde{E}(r)$ (where $E(r) = \sqrt{\varepsilon(r)} E(r)$) are the field patterns of the harmonic modes, and the

eigenvalues ($\frac{w^2}{c^2}$) are proportional to the squared frequencies of those modes.

And the Maxwell equations are the most important kernel of following calculation method (both PWE and FDTD).

2.2 Plane-wave expansion method

Photonic crystal band diagram is a dispersion relation between frequency ω and wave-vector k , the PWE has a substantial meaning for photonic crystal calculation. Just like the Schrodinger equation for electrons, the wave equation for light has an important role in photonic crystal. The solid physics tell us the electrons in Coulomb potential can be replaced by the dielectric constant potential **ε(r)** of light and given by

$$\varepsilon(r) = \sum_G \varepsilon_G e^{jG \bullet r} \quad \ldots\ldots\ldots\ldots\ldots\ldots\ldots\ldots\ldots\ldots\text{.2.8}$$

G vector is the reciprocal lattice vector in wave-vector space which was defined in solid physics. It is a linear combination by Fourier expansion of fundamental frequency vector. The basic reciprocal vector has a relation with real lattice vectors *R*, the wave-vector *R* that we know is *primitive lattice vectors*. $R = la \hat{x} + mba \hat{y} + nc \hat{z}$, where (l, m, n) are integers. And we

general call primitive lattice vectors a_1, a_2, and a_3, they don't need to be unit length. Then the reciprocal vectors mentioned above, $\boldsymbol{G}$, where the reciprocal vectors also have a set of primitive reciprocal vectors, b_1, b_2, b_3 ,$\boldsymbol{G}=l\,b_1+m\,b_2+n\,b_3$, and the $\vec{G}\bullet\vec{R}=2N\pi$, among this definition , $a_{i*}b_j=2\pi$, if i =j or 0 ,if i≠j .so we can get the reciprocal vectors ,

$$b_1 = 2\pi\,\frac{a_2 \times a_3}{a_1 \cdot a_2 \times a_3}$$

$$b2 = 2\pi\,\frac{a3 \times a_1}{a_1 \cdot a_2 \times a_3}$$

$$b_13 = 2\pi\,\frac{a_1 \times a2}{a_1 \cdot a_2 \times a_3} \qquad \dots\dots\dots\dots\dots\dots\dots\dots\dots\dots\dots\dots\dots.2.9$$

Fig. 2.1 show the real space and reciprocal vectors in triangular photonic crystal structure, The real space, the lattice constant is *a*. In reciprocal space, $R_1 \bullet G_1 = 2\pi, R_2 \bullet G_2 = 2\pi, R_1 \bullet G_2 = 0, R_2 \bullet G_1 = 0$, fig. 2.1 clearly present it.

Real space   reciprocal lattices space

$$R_1 \bullet G_1 = 2\pi$$
$$R_2 \bullet G_2 = 2\pi$$
$$R_1 \bullet G_2 = 0$$
$$R_2 \bullet G_1 = 0$$
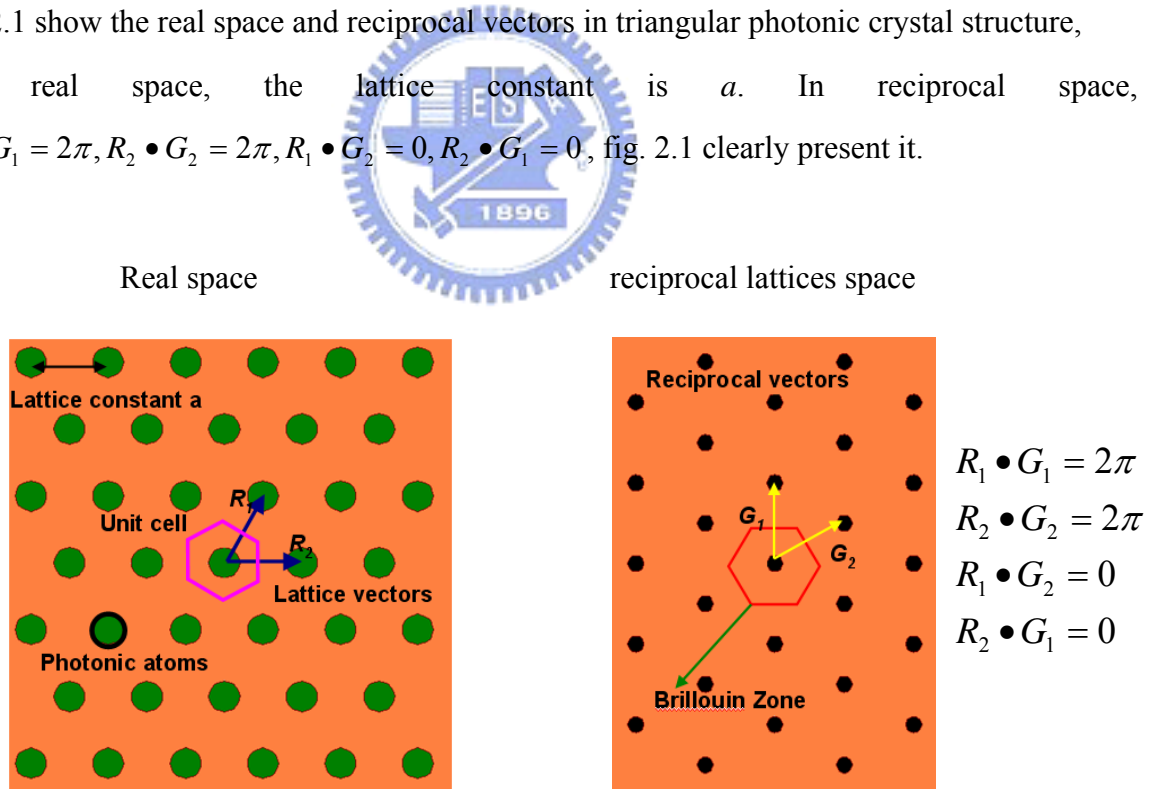
Fig. 2.1 The triangular photonic crystal structure and its reciprocal space and real space.

To calculate the propagation in periodically structure, we can describe the wave function as

$$\Phi(r) = \sum_G \Phi_G e^{j(G+k)\bullet r}$$ ……………………………………2.10

Where the **k** is arbitrary vector, but when it is larger than **G/2, k** can be change with **k-G** , and the result will not change. Consequently if the **k** value is large than **G** vector, it can exchange a vector **k-G** in the Brillouin Zone. Then the equation 2.9 、2.10 can substituted into the wave function for electric field **E** (2.6) or the magnetic field **H** (2.7). Then we can get the new equation.

$$\nabla \times [\nabla \times E(r,t)] = \omega^2 \varepsilon(r) E(r,t) \rightarrow (k+G)\bullet(k+G') \times E_{G'} = -\omega^2 \sum_{G'} \varepsilon_{G,G'} E_{G'}$$ ………... 2.11

$$\nabla \times [\frac{1}{\varepsilon(r)}\nabla \times H(r,t)] = \omega^2 H(r,t) \rightarrow (k+G) \times \sum_{G'} \varepsilon^{-1}{}_{G,G'}(k+G')H_{G'} = -\omega^2$$ ………… 2.12
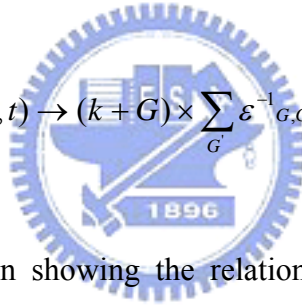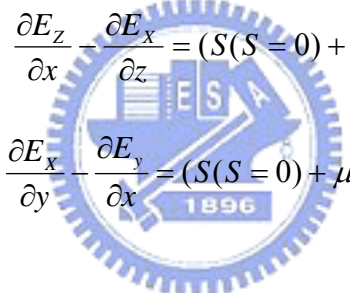
These are matrix equation showing the relation between **ω** and **k,** where $\varepsilon_{G,G'}$ and $\varepsilon^{-1}{}_{G,G'}$ are the Fourier coefficient matrices of **ε(r)** and **ε(r)$^{-1}$**.By solving the one of these two equation, we can get the dispersion relation , and this method is based on Fourier expansion to solve the electromagnetic wave in the material called Plane wave expansion . in these thesis, the band diagrams of photonic crystal which made by this way.

2.3 Finite difference time domain method

Generally to solve the electromagnetic light in space and time changes, the numerical method Finite difference time domain (FDTD) is always been chosen. FDTD use the finite difference method but put the term of time in the calculation. In this method, the object in the finite space would divide into many cubic cell, the cell is called Yee's cell, and the Δ x, Δ y, Δ z are the same length. Then in Maxwell's equations, integral the electric and magnetic field in

x, y ,z direction with short time Δ t.

In order to simplify the Maxwell equation to conveniently process the calculation, the divergent formula of 2.1 for electric and magnetic field would rewrite. Then we change the formula 2.1 to another form.

$$\frac{\partial H_Z}{\partial y} - \frac{\partial H_Y}{\partial z} = (\sigma + \varepsilon \frac{\partial}{\partial t})E_X$$

$$\frac{\partial H_X}{\partial z} - \frac{\partial H_Z}{\partial x} = (\sigma + \varepsilon \frac{\partial}{\partial t})E_Y$$

$$\frac{\partial H_Y}{\partial x} - \frac{\partial H_X}{\partial y} = (\sigma + \varepsilon \frac{\partial}{\partial t})E_Z$$

$$\frac{\partial E_Y}{\partial z} - \frac{\partial E_Z}{\partial y} = (S(S=0) + \mu \frac{\partial}{\partial t})H_X$$

$$\frac{\partial E_Z}{\partial x} - \frac{\partial E_X}{\partial z} = (S(S=0) + \mu \frac{\partial}{\partial t})H_Y$$

$$\frac{\partial E_X}{\partial y} - \frac{\partial E_Y}{\partial x} = (S(S=0) + \mu \frac{\partial}{\partial t})H_Z \dots \dots \dots \dots \dots 2.13$$

But the magnetic loss (S) doesn't consider in the Maxwell equation. The six equations become the complete three dimensional problem, practical discussions of the propagation of light always along one-axis, two-axis, three-axis and let variation of z-axis equal to zero if the wave propagate along z-axis, variation of y-axis to be zero along y-axis, variation of z-axis to be zero along z-axis. Then the polarization direction of electric field or magnetic field can be treat as TE, TM or TEM mode.

Yee first use the concept of cell to describe the Maxwell's equation, utilize the short distance $\Delta x, \Delta y, \Delta z$ to present the length of three-axis , and the Δt to describe the increase of time. The coordinate of cell (x, y, z) can mark as $(i, j, k) = (i\Delta x, j\Delta y, k\Delta z)$, and the space function correspond to time can write $F^n(i, j, k) = F(i\Delta x, j\Delta y, k\Delta z, n\Delta z)$, and i ,j ,k, n are integral. And the difference equation of space and time can write as

$$\frac{\partial F^n(i,j,k)}{\partial x} = \frac{F^n(i+1/2,j,k) - F^n(i-1/2,j,k)}{\Delta x} + o(\Delta x^2)$$

$$\frac{\partial F^n(i,j,k)}{\partial t} = \frac{F^{n+1/2}(i,j,k) - F^{n-1/2}(i,j,k)}{\Delta t} + o(\Delta t^2) \dots\dots\dots\dots\dots 2.14$$

In the Yell cell, the magnetic field is slower half time step than electric field, consider the fig. 2.2, we re-write the formula 2.13 and we can get the $H_x^{n+1}, H_y^{n+1}, H_z^{n+1}, E_x^{n+1}, E_y^{n+1}, E_z^{n+1}$.
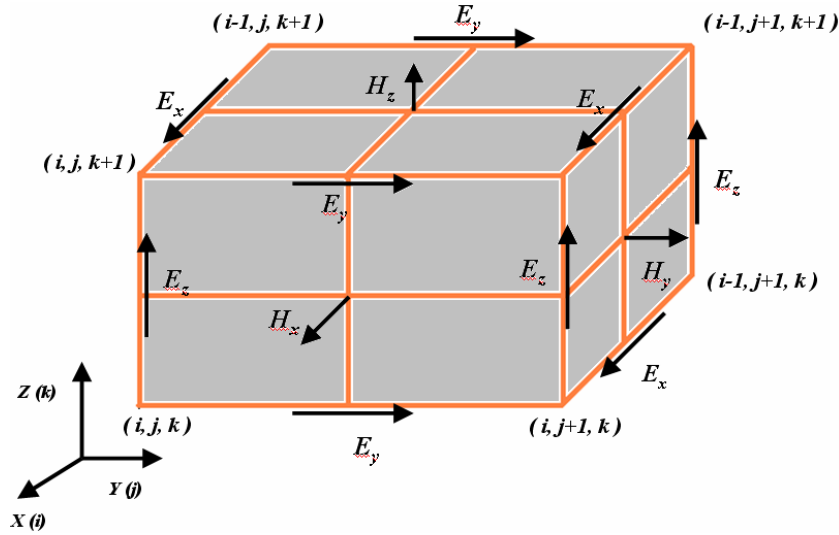

Fig. 2.2 The Yell cell of a calculation modal of FDTD method

$$E_x^{n+1}(i+1/2,j,k) = C_x(i+1/2,j,k)\{-D_x(i+1/2,j,k)E_x^n(i+1/2,j,k)$$
$$+\frac{H_z^{n+1}(i+1/2,j+1/2,k) - H_z^{n+1}(i+1/2,j-1/2,k)}{\Delta y}$$
$$-\frac{H_x^{n+1}(i+1/2,j,k-1/2) - H_x^{n+1}(i-1/2,j,k-1/2)}{\Delta z}\}\dots\dots\dots\dots\dots 2.15$$

$$E_y^{n+1}(i,j+1/2,k) = C_y(i,j+1/2,k)\{-D_y(i+1/2,j,k)E_y^n(i,j+1/2,k)$$
$$+\frac{H_x^{n+1}(i,j+1/2,k+1/2) - H_x^{n+1}(i,j+1/2,k-1/2)}{\Delta z}$$
$$-\frac{H_x^{n+1}(i+1/2,j+1/2,k) - H_x^{n+1}(i-1/2,j+1/2,k)}{\Delta x}\}\dots\dots\dots\dots\dots 2.16$$

$$E_z^{n+1}(i,j,k+1/2) = C_z(i,j,k+1/2)\{-D_z(i,j,k+1/2)E_z^n(i,j,k+1/2)$$

$$+\frac{H_y^{n+1}(i+1/2,j,k+1/2)-H_y^{n+1}(i-1/2,j,k+1/2)}{\Delta x}$$

$$-\frac{H_x^{n+1}(i,j+1/2,k+1/2)-H_x^{n+1}(i,j-1/2,k+1/2)}{\Delta y}\}\dots\dots\dots\dots\dots\dots 2.17$$

$$H_x^{n+1}(i,j+1/2,k+1/2) = C_x^{'}(i,j+1/2,k+1/2)\{-D_x^{'}(i,j+1/2,k+1/2)H_x^{n-1/2}(i,j+1/2,k+1/2)$$

$$+\frac{E_y^n(i,j+1/2,k+1)-E_y^n(i,j+1/2,k)}{\Delta z}$$

$$-\frac{E_z^n(i,j+1,k+1/2)-E_z^n(i,j,k+1/2)}{\Delta y}\}\dots\dots\dots\dots\dots\dots\dots\dots\dots 2.18$$

$$H_y^{n+1}(i+1/2,j,k+1/2) = C_y^{'}(i+1/2,j,k+1/2)\{-D_y^{'}(i+1/2,j,k+1/2)H_y^{n-1/2}(i+1/2,j,k+1/2)$$

$$+\frac{E_x^n(i+1/2,j,k+1)-E_x^n(i+1/2,j2,k)}{\Delta z}$$

$$-\frac{E_z^n(i+1/2,j,k+1)-E_z^n(i+1/2,j,k)}{\Delta z}\}\dots\dots\dots\dots\dots\dots\dots\dots\dots 2.19$$

$$H_z^{n+1}(i+1/2,j+1/2,k) = C_z^{'}(i+1/2,j+1/2,k)\{-D_z^{'}(i+1/2,j+1/2,k)H_z^{n-1/2}(i+1/2,j+1/2,k)$$

$$+\frac{E_z^n(i+1/2,j+1,k)-E_z^n(i+1/2,j,k)}{\Delta y}$$

$$-\frac{E_x^n(i+1,j+1/2,k)-E_x^n(i,j+1/2,k)}{\Delta x}\}\dots\dots\dots\dots\dots\dots\dots\dots\dots 2.20$$

In the six formulas, the C_u, D_u, $C_u^{'}$, $D_u^{'}$ are identified as

$$C_u(i,j,k) = \{\sqrt{\frac{\mu_0}{\varepsilon_0}}\cdot(\frac{\sigma_u(i,j,k)}{2}+\frac{\varepsilon_u(i,j,k)}{\Delta t})\}^{-1}$$

$$D_u(i,j,k) = \{\sqrt{\frac{\mu_0}{\varepsilon_0}}\cdot(\frac{\sigma_u(i,j,k)}{2}-\frac{\varepsilon_u(i,j,k)}{\Delta t})\}$$

$$C_u^{'}(i,j,k) = \{\sqrt{\frac{\mu_0}{\varepsilon_0}}\cdot(\frac{s_u(i,j,k)}{2}+\frac{u_u(i,j,k)}{\Delta t})\}^{-1}$$

$$D_u^{'}(i,j,k) = \{\sqrt{\frac{\mu_0}{\varepsilon_0}}\cdot(\frac{s_u(i,j,k)}{2}-\frac{u_u(i,j,k)}{\Delta t})\}\dots\dots\dots\dots\dots\dots 2.21$$

The formulas mentioned above are the three-dimensional FDTD description, it can be seen that any time step, the electric and magnetic fields can be decided as by three factor, one is the electric and magnetic filed last time step, second, for electric field the magnetic fields around the electric field at the same time step, for magnetic field are the electric fields around it, third, the coefficient of the σ and μ.

When we use the FDTD method, an important problem is the stability of solution, the more significant factor is Δt, the relation of short time step between short distance $\Delta x, \Delta y, \Delta z$ is very critical to the simulation. Now, we consider the free source problem, s and σ equal to zero. Using the two divergent formulas form 2.4, we get $j\nabla \times (H + jE) = 0$, and let $H + jE = V$, we get the eigen-value problem.

$$\frac{\partial V}{\partial t} = \lambda V = jc\nabla \times V \quad \text{………………………………………}2.22$$

Identified the $V^{n+1}/V_n = q$, put q into formula 2.22, we can get q.

$$q = \lambda \frac{\Delta t}{2} \pm \sqrt{1 + (\lambda \frac{\Delta t}{2})^2} \quad \text{……………………………………}2.23$$

Because the stability of the calculation the $|q| \leqq 1$, and get Re(λ)=0, Im(λ)≦2/△t. Then we

assume $V = V_0 e^{(j(lk_x \Delta x + mk_y \Delta y + nk_z l\Delta z)}$ put into 2.14 to get
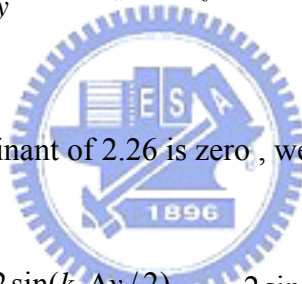
$$\frac{\partial}{\partial x} = \frac{j2\sin(k_x \Delta x / 2)}{\Delta x}$$
$$\frac{\partial}{\partial y} = \frac{j2\sin(k_y \Delta x / 2)}{\Delta y}$$
$$\frac{\partial}{\partial z} = \frac{j2\sin(k_z \Delta z / 2)}{\Delta z} \quad \text{………………………………………………………………}2.24$$

Then the formula $\dfrac{\partial V}{\partial t} = \lambda V = jc \nabla \times V$ become to

$$-2c\left(\frac{j2\sin(k_x\Delta x/2)}{\Delta x}, \frac{j2\sin(k_y\Delta y/2)}{\Delta y} \frac{j2\sin(k_z\Delta z/2)}{\Delta z}\right) \times V(l,m,n) = \lambda V(l,m,n) .... 2.25$$

we divided into three parts by x, y, z direction, we get

$$-\frac{2c\sin(k_y\Delta y/2)}{\Delta y}V_z + \frac{2c\sin(k_z\Delta z/2)}{\Delta z}V_y = \lambda V_x$$

$$-\frac{2c\sin(k_z\Delta z/2)}{\Delta z}V_x + \frac{2c\sin(k_x\Delta x/2)}{\Delta x}V_z = \lambda V_y$$

$$-\frac{2c\sin(k_x\Delta x/2)}{\Delta x}V_y + \frac{2c\sin(k_y\Delta y/2)}{\Delta y}V_x = \lambda V_z .... 2.26$$

The only solution is the determinant of 2.26 is zero , we can get λ

$$\lambda = -4c^2\left[\left(\frac{2\sin(k_x\Delta x/2)}{\Delta x}\right)^2 + \left(\frac{2\sin(k_y\Delta y/2)}{\Delta y}\right)^2 + \left(\frac{2\sin(k_z\Delta z/2)}{\Delta z}\right)^2\right] .... 2.27$$

We get $\mathrm{Re}(\lambda)=0$ and $\mathrm{Im}(\lambda) \le 2c\sqrt{\dfrac{1}{\Delta x^2} + \dfrac{1}{\Delta y^2} + \dfrac{1}{\Delta z^2}}$, then $2c\sqrt{\dfrac{1}{\Delta x^2} + \dfrac{1}{\Delta y^2} + \dfrac{1}{\Delta z^2}} \le \dfrac{2}{\Delta t}$,

So the stability condition of time step has proof as

$$C_{Max}\Delta t \le \left(\frac{1}{\Delta x^2} + \frac{1}{\Delta y^2} + \frac{1}{\Delta z^2}\right)^{-1} .... 2.28$$

Chapter 3 Simulation results and analysis

3.1 Characteristics of line-defect photonic crystal waveguides

In this thesis, high transmission an broad-band photonic crystal waveguide will be studied. Before starting to discuss the structure of our design, the characteristics of photonic crystal waveguide is presented. First, epi-structure shown as InP-**In$_{0.74}$Ga$_{0.26}$As$_{0.54}$P$_{0.46}$**-InP (substrate), the structure is fig. 3.1
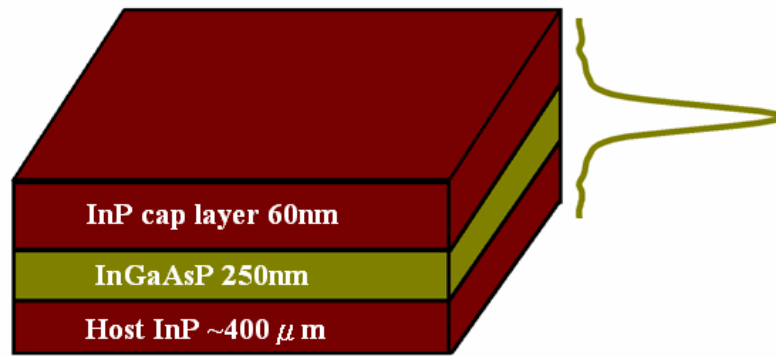

Fig. 3.1 The Epitaxial Structure of design structure.

To make sure that the electromagnetic wave in guide layer (InGaAsP layer) is fundamental mode, the thickness of guide layer design to be 250nm, the finite-difference method is used to calculate the thickness. This can be treated as one-dimensional problem to solve, the formula to calculate TE mode polarization in the structure is equation 3.1.

$$
\begin{bmatrix}
(n_1^2 - \dfrac{2}{\Delta x^2}) & \dfrac{1}{\Delta x^2} & 0 & 0 \\
\dfrac{1}{\Delta x^2} & (n_1^2 - \dfrac{2}{\Delta x^2}) & \dfrac{1}{\Delta x^2} & 0 \\
0 & 0 & \ddots & 0 \\
0 & 0 & \dfrac{1}{\Delta x^2} & (n_I^2 - \dfrac{2}{\Delta x^2})
\end{bmatrix}
\begin{bmatrix} U_1 \\ U_2 \\ \vdots \\ U_4 \end{bmatrix}
= n^{-2}
\begin{bmatrix} U_1 \\ U_2 \\ \vdots \\ U_4 \end{bmatrix}
$$
..................................3.1

But the waveguide will be undercut, the InP under the InGaAsP layer will be removed, then the InGaAsP layer become a membrane. The TE wave in the epi-structure is in fig. 3.2, in fig. 3.2 the simulation structure is air-InGaAsP-air. Then we also get the effective index 2.8 for the membrane structure (air - InGaAsP - air) and the confining factor is 0.877.
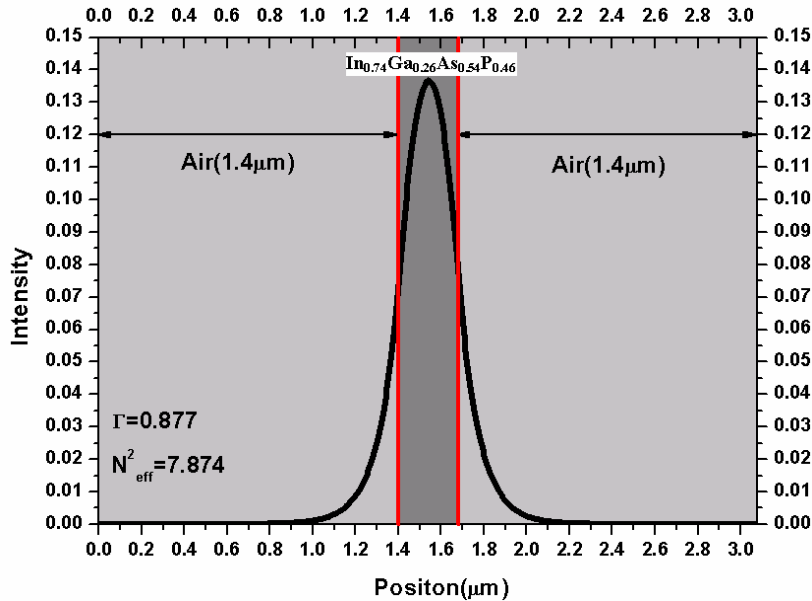

Fig. 3.2 The distribution of fundamental mode is shown.

In order to simulate the photonic crystal waveguide, it is important that the range of the communicated wavelength is about 1550nm for TE mode. In our design, first the radius of air holes and lattice constant between holes and holes become very critically. In the photonic crystal waveguide, finally the radius is 150nm and period is 465nm, the band-structure has no defect is fig. 3.3, the forbidden band is from $0.2647(\lambda/\Lambda)$ to $0.346(\lambda/\Lambda)$, the forbidden band is around 1550nm.
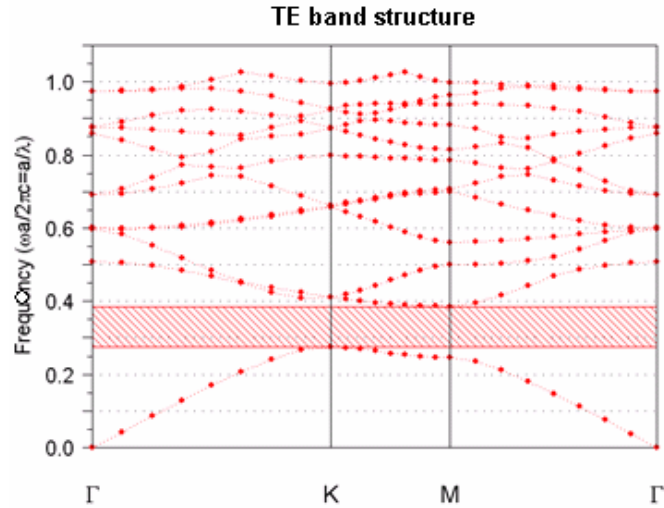
TE band structure

Fig. 3.3 The TE mode band structure of r=150nm, a=465nm photonic crystal has no defect.

Then taking one row of air holes off and simulate the band structure along Γ-K direction, we can get the defect mode in forbidden band. The defect modes have two modes, one is even mode and another is odd mode. In fig 3.3 we can clearly see the defect mode in line-defect photonic crystal. The line-defect photonic crystal waveguide have even and odd modes, even mode is form D to A, and the odd mode is for C-D, in fig. 3.5, Fig. 3.6 the field intensity of A, B, C, D propagation mode are shown. In the defect mode, the even mode is from 0.270~0.360(Λ/λ), the transmission spectrum is shown in fig. 3.7 (a) ,odd mode is form 0.295~0.315(Λ/λ), the transmission spectrum is shown in fig. 3.7 (b).
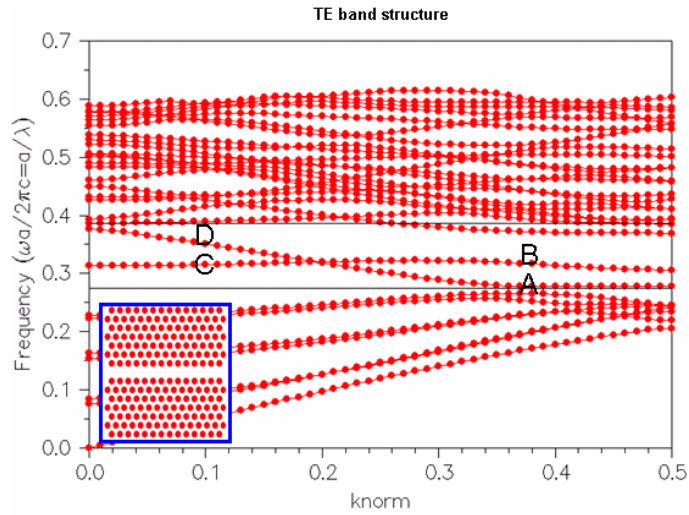
Fig. 3.4 The TE mode band structure of r=150nm, a=465nm line-defect photonic crystal
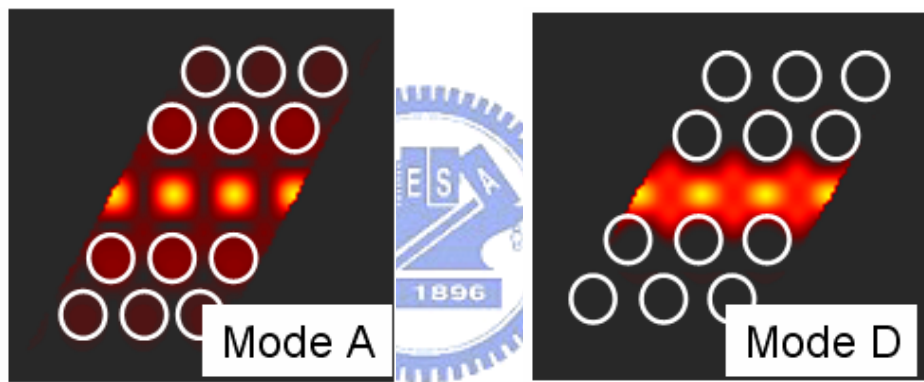
Fig. 3.5 The intensity of filed distribution of mode A and mode D , so the even mode is from

mode A to mode D
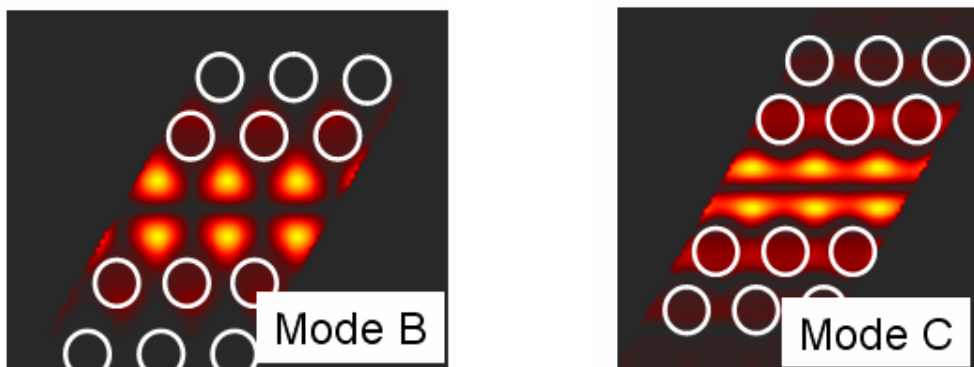
Fig. 3.6 The intensity of filed distribution of mode B and mode C , so the even mode is from
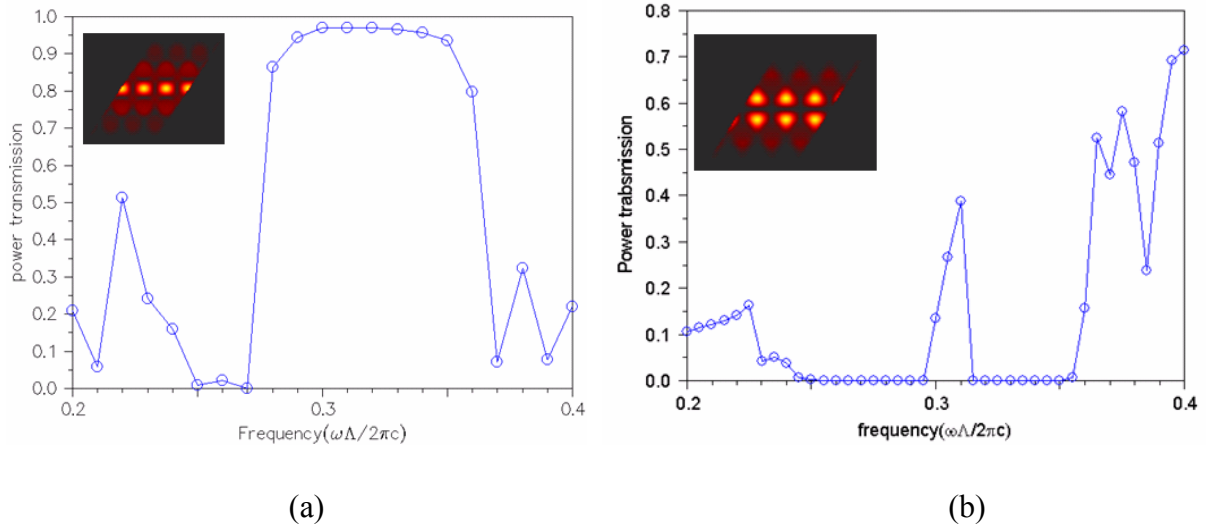
mode C to mode B

| (a) | (b) |

Fig. 3.7 (a) The even mode transmission spectrum. (b) The odd mode transmission spectrum.

There are two things to be considered in our photonic crystal structure, first is the thickness of InGaAsP layer and the fundamental mode in the membrane waveguide. Second, the transmission spectrum of photonic crystal waveguide is around 1550nm TE wave and broad-band is even mode. In later parts, the input light is considered as fundamental mode and also in photonic crystal waveguide.

3.2 Conventional double 60^0-bend and 120^0-bend photonic crystal waveguides

In this part, the sample double 60^0-bend and 120^0-bend photonic crystal waveguides are discussed and double 60^0-bend photonic crystal waveguide is first. In photonic crystal design, the radius of air holes is 150nm, the lattice constant is 465nm, the effective index is 2.8 for InGaAsP membrane structure, the air holes are removed to form a conventional double 60^0-bend waveguide in fig. 3.8(a), the transmission spectrum is in fig. 3.8(b). The transmission spectrum is very bad for this conventional structure.
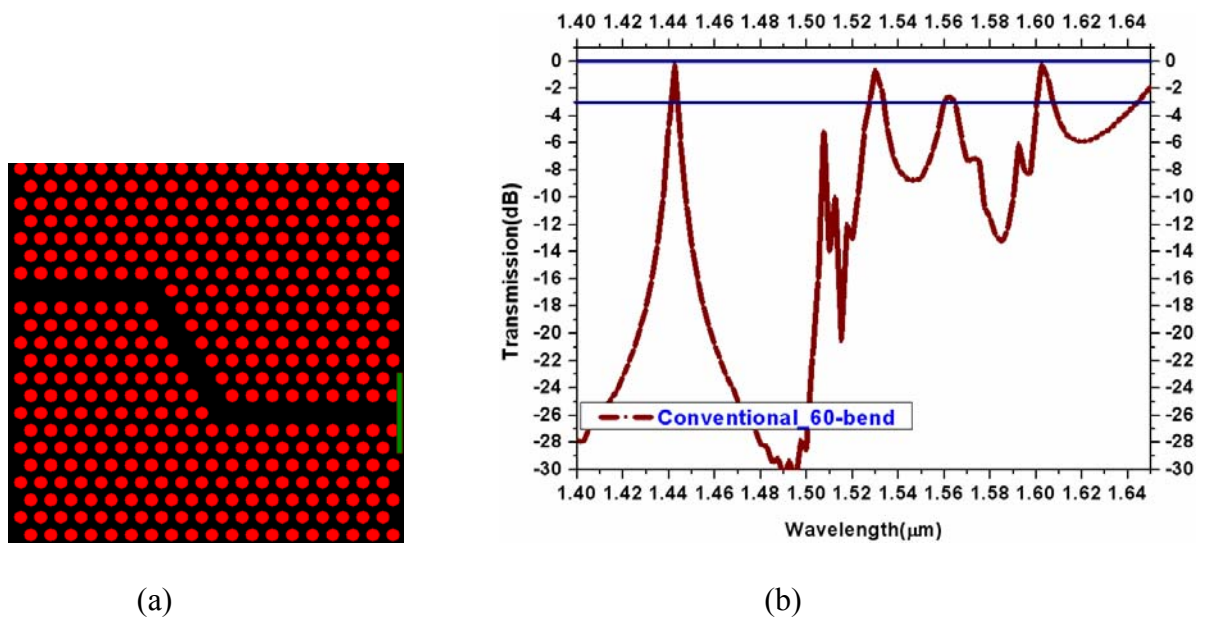
(a)   (b)

Fig. 3.8 (a) The conventional double-60^0 bend photonic crystal waveguide structure (b) Transmission spectrum of the conventional double 60^0-bend photonic crystal waveguide.

In conventional double 120^0-bend air holes are removed, especially at bend region, there are three ways to change the arrangement of air holes. The three bend type is shown in fig. 3.9, form left to right is type A, type B, type C. fig. 3.10 is the transmission spectrum of these three type conventional 120^0-bend PCWG. From the transmission spectrum, these types don't have significant band around 1.55um and loss are all very high. The improvement of the transmission in double 60^0-bend and double 120^0-bend is our research topics, and the design and simulation are introduced in chapter 3.3
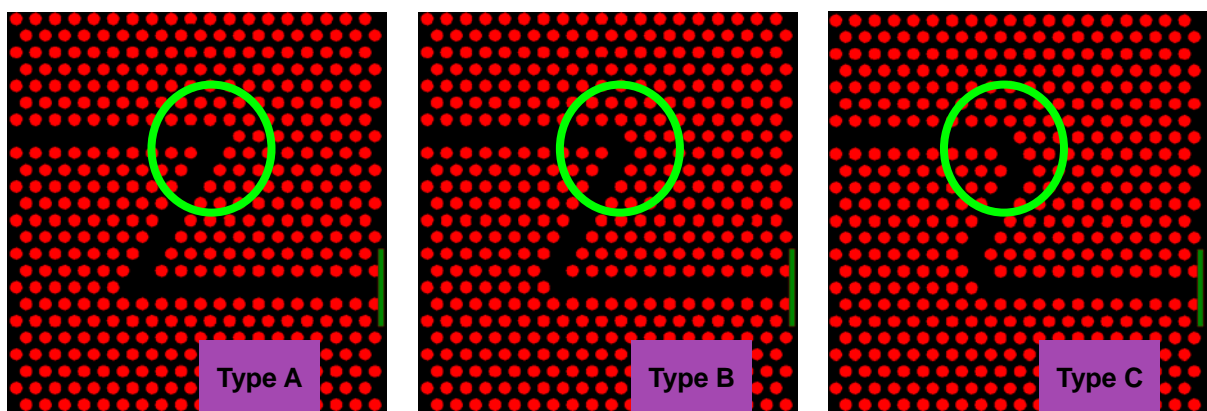
Fig. 3.9 Three type for double 120^0-band conventional photonic crystal waveguides, form left to right is type A, type B, type C.
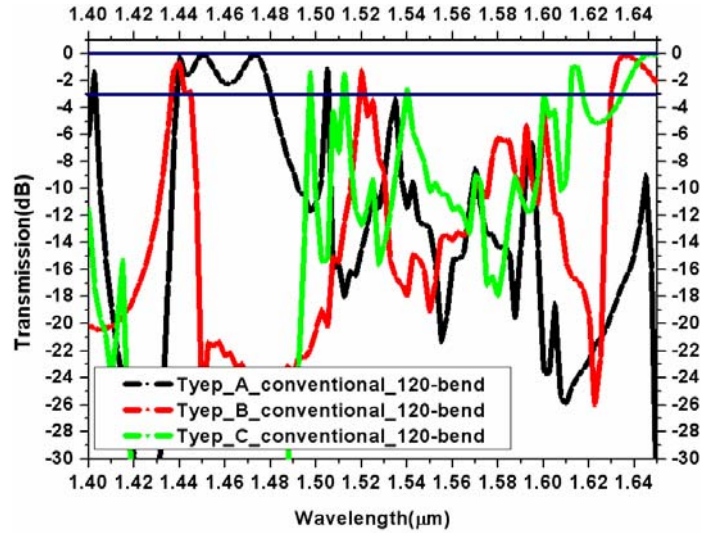
Fig. 3.10 The transmission spectrum for three conventional type double 120^0-bend photonic

crystal waveguides.

3.3 Using planer mirrors at bend region to improve transmission bandwidth of 60^0 and 120^0 bend waveguides

The photonic crystal waveguide structure is assumed to be defined in InGaAsP with a refractive index of 3.42, and the effective index is 2.8. The lattice constant Λ of the triangular lattice photonic crystal is 0.465 μm and the air-hole radius is 0.15 μm. The photonic band gap for this lattice is from $0.2477(\lambda/\Lambda)$ to $0.38595(\lambda/\Lambda)$ in normalized frequency, which corresponds to 1.20μm~1.87μm in wavelength. In order to improve the transmission of double-60°-bend photonic crystal waveguides, generally tuning the air holes near the bend region is employed. Here we don't change the shapes or positions of air holes at the bend region. Instead we try to dig a rectangular hole at the 60°-bend and 120^0-bend region as a planer mirror for total internal reflection to reform the transmission spectra.

3.3.1 Increasing or decreasing the width of the rectangular mirror on both sides or one side of 60⁰-bend photonic crystal waveguide

In our design, two planer mirrors are embedded at the double-60°-bend regions. The width of the rectangular mirror is the same as the diameter of the air holes. The illustration of the structure is shown in fig. 3.11 (a) for one bend. From the transmission spectrum, transmission above -3dB for wavelength from 1.48 μm to 1.52 μm can be obtained. The total bandwidth is 50 nm. The planar mirror added at the 60°bend region had been reported before by Miao et al., but their results are not optimized. Further improvement can be made by tuning the width of the mirror. The width of the mirror at the bend region has huge influence on the transmission characteristic. When light propagates through the 60°-bend region, the transmission and reflection will cause Fabry-Perot interferences. Mirror with certain widths can be expected to get better transmission. So we vary the width of the mirror in two ways. The first one is uniformly increasing or decreasing the width of the rectangular mirror on both sides as shown in fig. 3.11 (b), and we call this "Type A". The second one shown in fig. 3.11 (c) is by keeping the side of the mirror closer to the waveguide channel at the same position; we vary the width of the mirror by changing the position of the other side of the mirror. We call this "Type B".

(a)   (b)   (c)
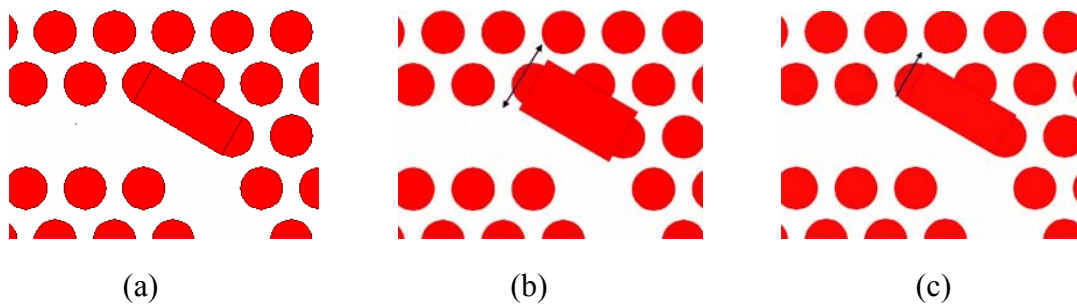
Fig. 3.11 Three different mirror structures simulated for double-60°-bend PCWGs. (a) The width of the planer mirror added at the bend region is the same as the diameter of air holes, which is 300 nm. (b) Type A: the width of the mirror is varied for both sides of the mirror. (c) The width of the mirror is varied for only one side of the mirror.

In type A, rectangular mirrors are added at bend region and to simulate the transmission spectra per 20nm increase from the width of mirror is 200nm. The transmission spectra are shown in fig. 3.12~ fig. 3.14 and the bandwidth is in Table 1, the transmission (dB) is defined by the formula $10*log(P_{out}/P_{in})$. P_{out} is the output intensity of our design waveguides, P_{in} is output intensity of the reference waveguide which is a line defect waveguide. And the high transmission is defined the transmission >-3dB.

(a)   (b)
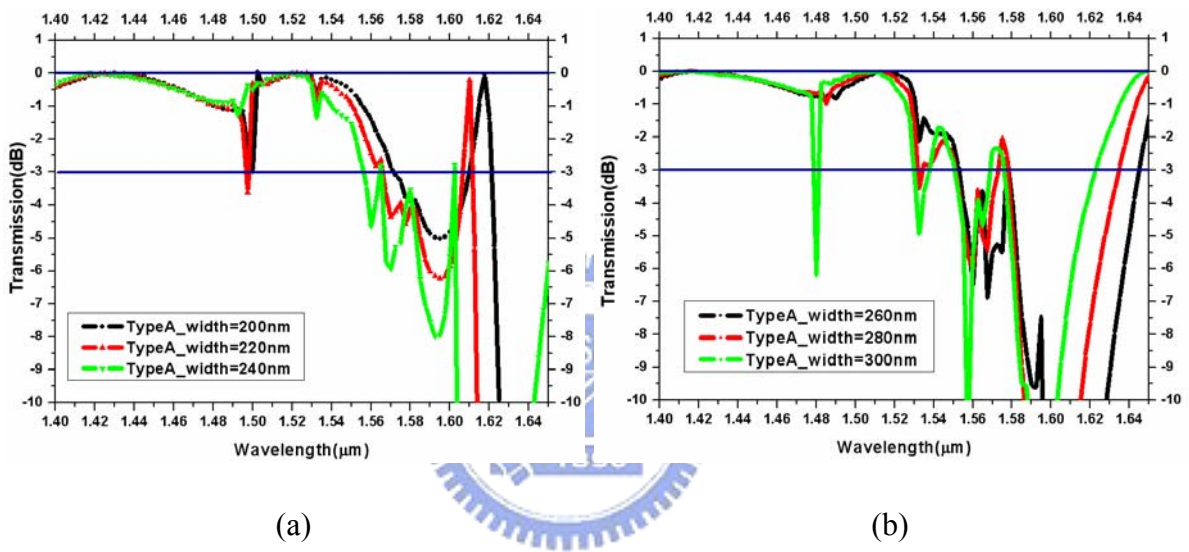
Fig. 3.12 (a) The width of mirrors are 200,220,240 nm in Type A (b) The width of mirrors are 260, 280, 300nm in Type A.

(a)   (b)
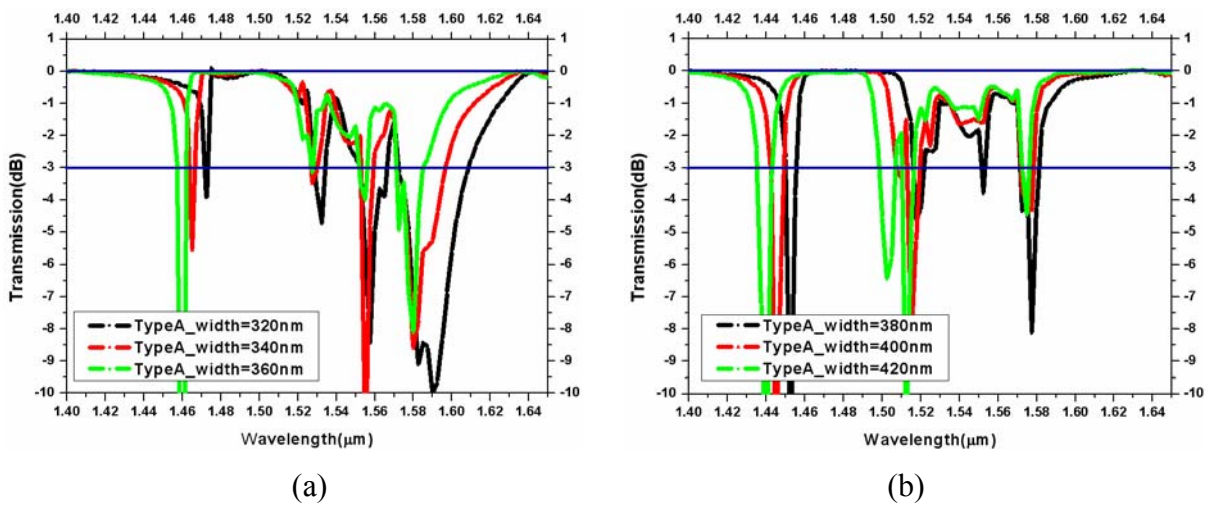
Fig. 3.13 (a) The width of mirrors are 320,340,360 nm in Type A (b) The width of mirrors are 380, 400, 420nm in Type A

.
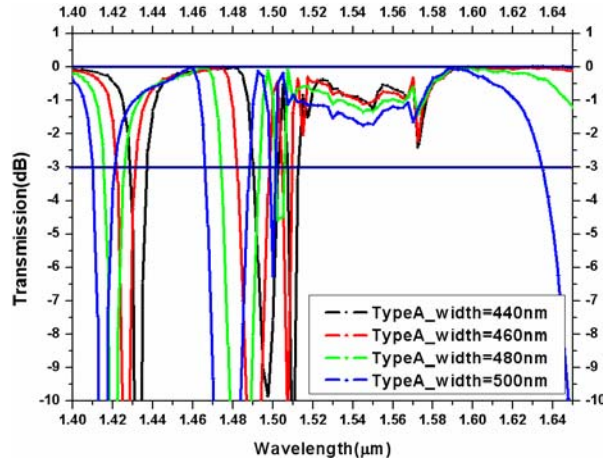
Fig. 3.14 The width of mirrors are 440,460,480,500nm in Type A

Table 1   Type A in double 60^0-bend

Mirror width (nm)	High transmission wavelength range (μm)	Transmission bandwidth (nm)
200	1.374μm~1.500μm	123nm
220	1.362μm~1.520μm	140nm
240	1.355μm~1.497μm	142nm
260	1.350μm~1.553μm	203nm
280	1.355μm~1.532μm	177nm
300	1.355μm~1.478μm	123nm
320	1.355μm~1.471μm	116nm
340	1.596μm~1.722μm	126nm
360	1.584μm~1.722μm	138nm
380	1.581μm~1.721μm	140nm
400	1.579μm~1.717μm	138nm

420	1.575μm~1.712μm	137nm
440	1.512μm~1.701μm	189μm
460	1.509μm~1.684μm	175nm
480	1.506μm~1.659μm	154nm
500	1.501μm~1.634μm	133nm

From the figures above, it can be found when width of mirrors is 440nm, the double 60^0-bend have broad-bend transmission spectra around 1.55μm. Although the width of mirrors is 240nm, 260nm has broad-bend transmission form 1.35μm ~ 1.556μm, but the range of high transmission wavelength included 1.55μm isn't too much, then we focus on the width of mirror is 440nm. The high transmission spectrum (>-3dB) is from 1.512μm~1.701μm for the width of mirrors are 440nm, the broad-band is 189nm and around 1.55μm. In fig. 3.15 high transmission spectrum is shown in fig. 3.15(a) and the TE light propagation situation at 1.55μm is shown in fig. 3.15(b).

(a)   (b)
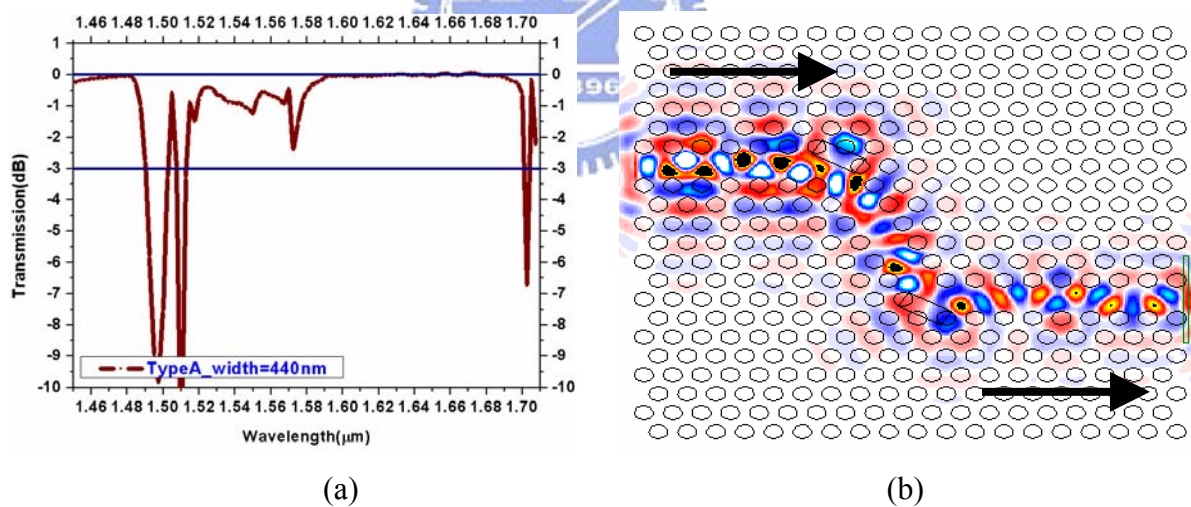
Fig. 3.15 (a) The transmission spectrum of the width of mirror is 440nm in Type-A (b) The TE field propagation at wavelength 1.55μm

In type B, planer mirrors are added at bend-region, but increase and decrease of the width is just for one-side to simulate the transmission spectra per 20nm increase from the width of mirror is 180nm. The transmission spectra are shown in fig. 3.16~ fig. 3.18 and the bandwidth is in Type 2
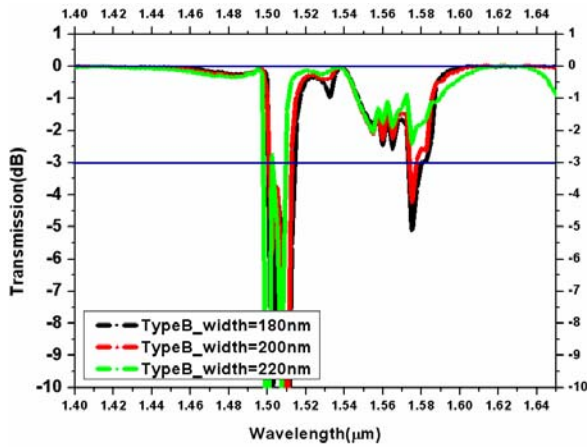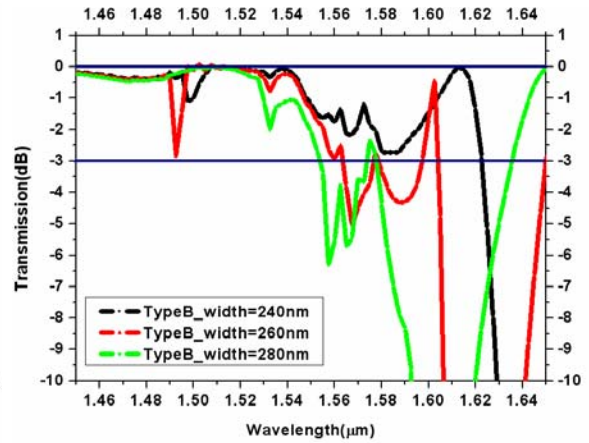
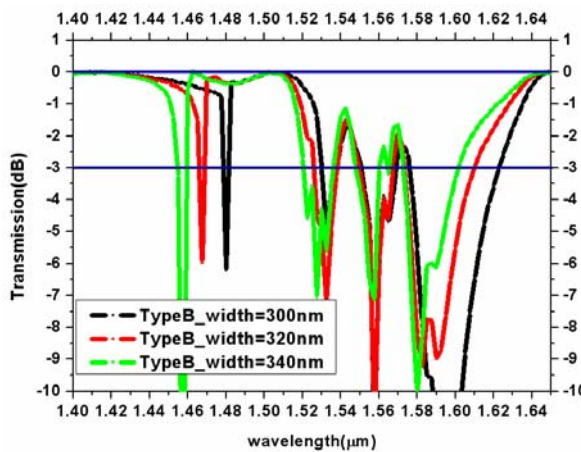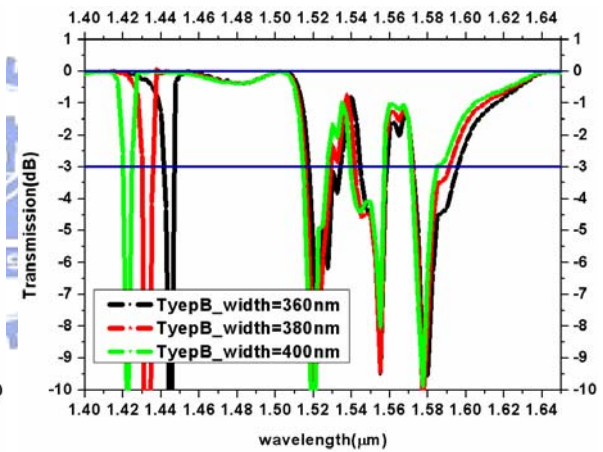(a)   (b)

Fig. 3.16 (a) The width of mirrors are 180,200,220 nm in Type B (b) The width of mirrors are

240,260,280nm in Type B.

(a)   (b)

Fig. 3.17 (a) The width of mirrors are 300,320,340 nm in Type B (b) The width of mirrors are
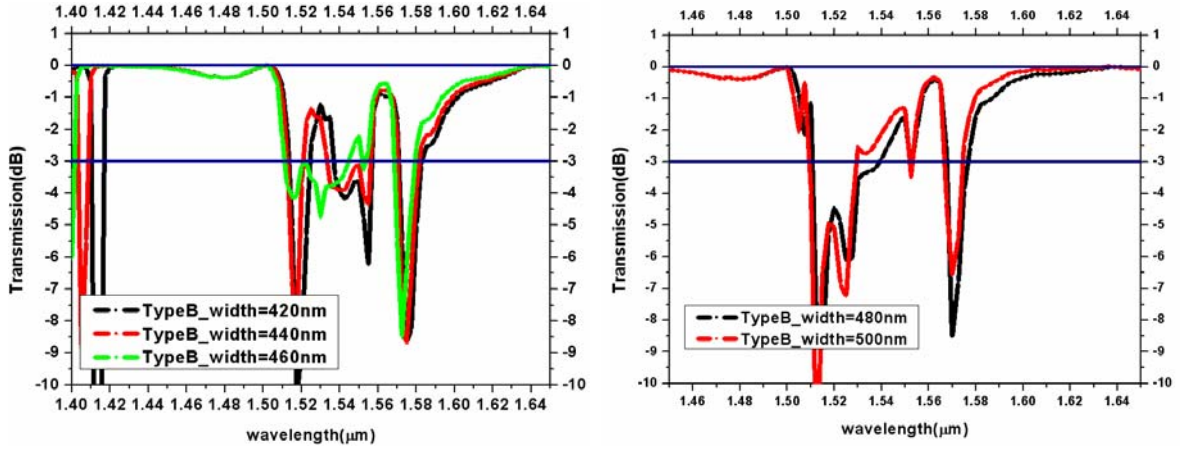
360,380,400nm in Type B.

Fig. 3.18 (a) The width of mirrors are420, 440, 460 nm in Type B, (b) The width of mirrors

are 480,500nm in Type B.

Table 2   Type B in double 60^0-bend

Mirror width (nm)	High transmission wavelength range (μm)	Transmission bandwidth (nm)
180	1.378μm~1.497μm	119nm
200	1.507μm~1.658μm	151nm
220	1.509μm~1.658μm	149nm
240	1.354μm~1.621μm	267nm
260	1.354μm~1.563μm	209nm
280	1.354μm~1.552μm	198nm
300	1.355μm~1.478μm	123nm
320	1.354μm~1.465μm	111nm
340	1.601μm~1.728μm	127nm
360	1.595μm~1.723μm	128nm
380	1.591μm~1.724μm	133nm
400	1.585μm~1.720μm	135nm
420	1.584μm~1.711μm	127nm
440	1.581μm~1.710μm	129nm
460	1.576μm~1.675μm	100nm

| 480 | 1.393μm~1.510μm | 117nm |
| 500 | 1.386μm~1.509μm | 123nm |

In these figures mention above when the width of mirrors is 240nm, the transmission spectrum is from 1.35μm to 1.622μm, the high transmission (>-3dB) band-width is exceed 272nm included 1.55μm, The transmission spectrum is shown in fig. 3.19(a) and the TE wave propagation situation at wavelength 1.55μm.
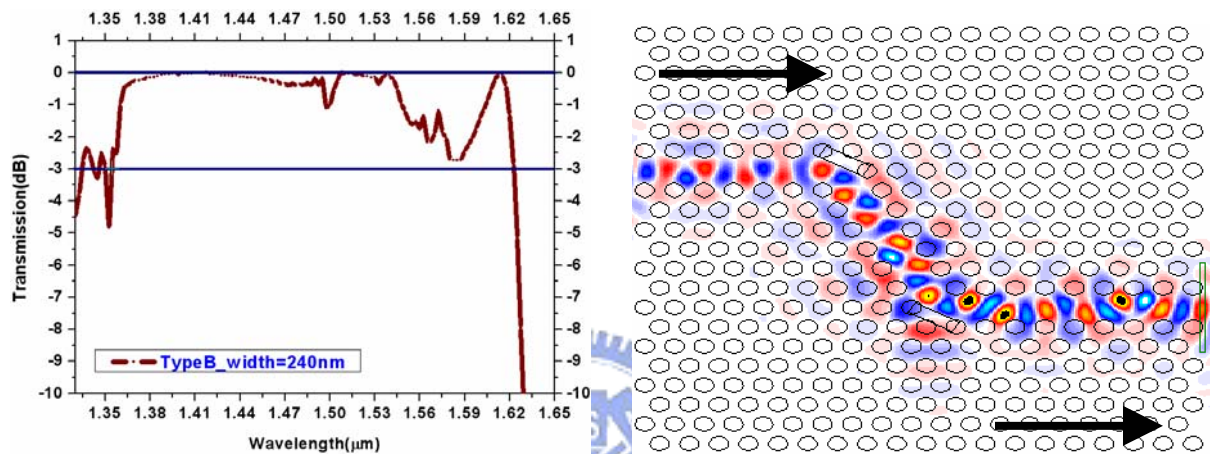

Fig. 3.19 (a) The transmission spectrum of the width of mirror is 240nm in Type-B (b) The TE field propagation at wavelength 1.55μm

In fig. 3.20 the bandwidth vs. the width of mirrors in Type A and Type B for double 60^0-bend PCWGs is shown.
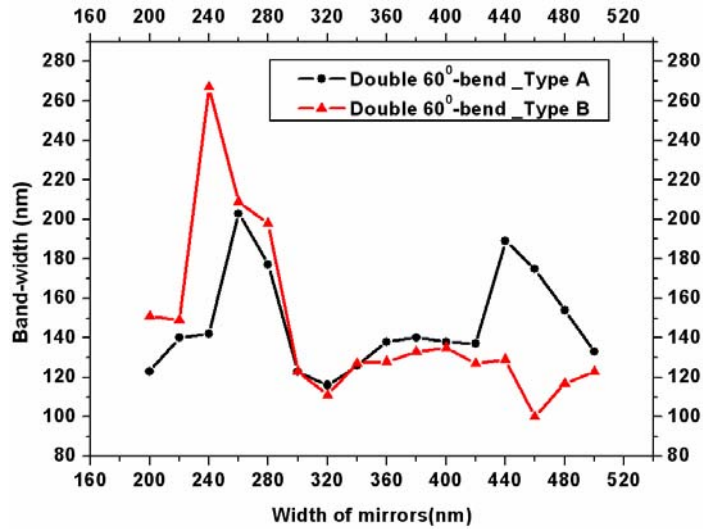
Fig. 3.20 The bandwidth vs. the width of mirrors in Type A and Type B for double 60^0- bend PCWGs

3.3.2 Increasing or decreasing the width of the rectangular mirror on both sides or one side of 120^0-bend photonic crystal waveguide

For double-$120°$-bend PCWG structures, we first add one planer mirror at the bend region as a reference, and then increase the number of mirrors to two and change their relative positions as shown in fig. 3.21 to obtain the optimized structure configurations. The three different structures considered are labeled Type I, Type II, and Type III. The transmission spectrum for each type is shown in fig. 3.22. We find that Type III has more potential for broadband transmission.
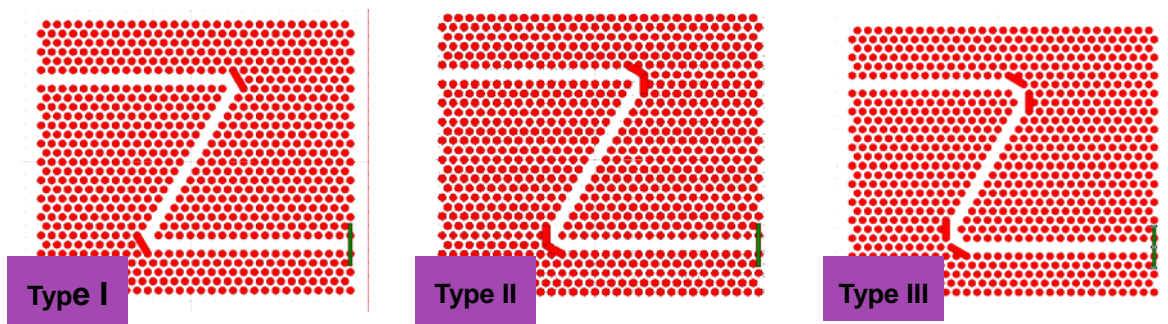
Fig. 3.21 Three different mirror structures for the design of high transmission broadband double-$120°$-bend PCWGs. The width of each mirror in the figure is 300 nm.
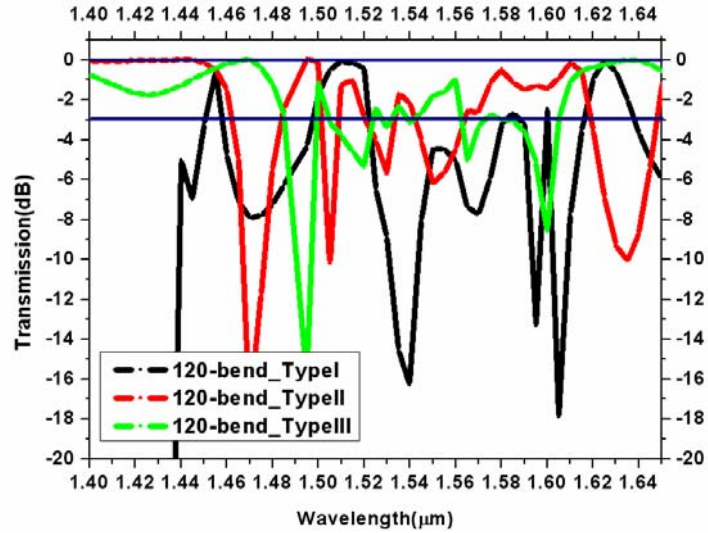
Fig. 3.22 Transmission spectra for Type I, Type II, and Type III for double-120°-bend photonic crystal waveguide.

To simulate double 120^0-bend photonic crystal waveguide, the planer mirrors are also utilized at bend region, the difference is that there are four mirrors to be used. Here are two types to increase or decrease the width of these four mirrors. Type A is that the mirrors increase or decrease both side, type B is that the four mirrors increase or decrease along one side and other side doesn't change. In type A, rectangular mirrors are added at 120^0-bend region and to simulate the transmission spectra per 20nm increased from the width of mirror is 200nm. The transmission spectra are fig. 3.23~ fig. 3.25, bandwidth is in Table 3 the transmission (dB) is used the formula $10*log(P_{out}/P_{in})$. P_{out} is the output intensity of design waveguide, P_{in} is output intensity of the reference waveguide which is a line defect waveguide. And the high transmission is defined the transmission >-3dB.
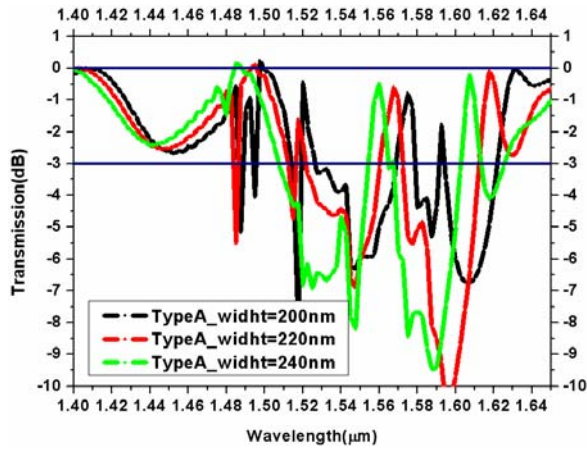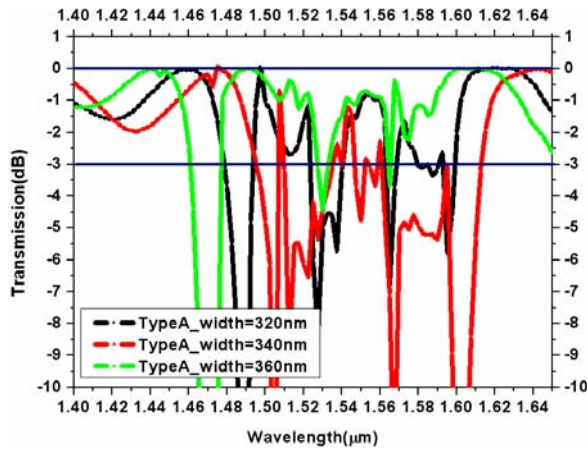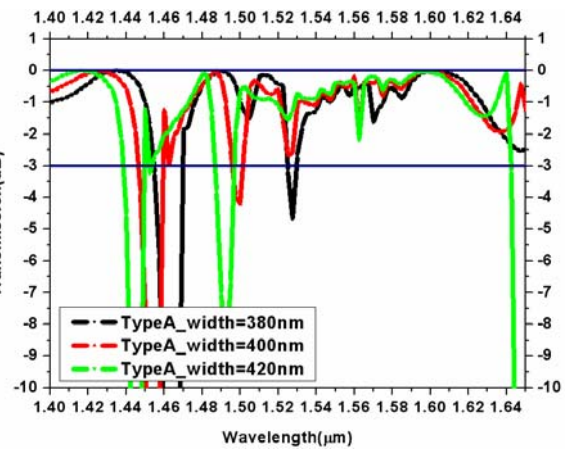
(a)
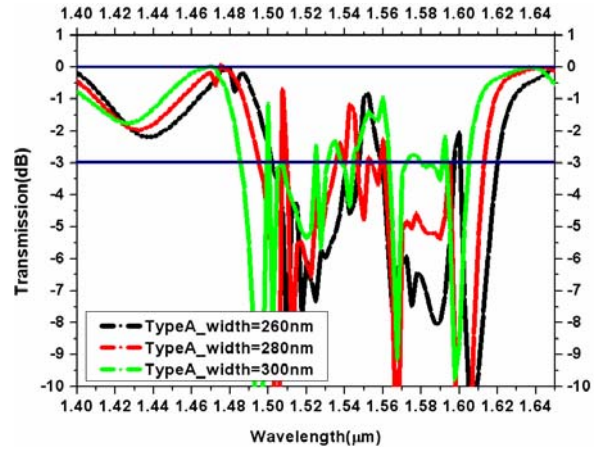
(b)

Fig 3.23 (a) The width of four mirrors are200, 220, 240 nm in Type A (b) The width of

mirrors are 260, 280, 300nm in Type A

(a)

(b)

Fig 3.24 (a) The width of four mirrors are200, 220, 240 nm in Type A (b) The width of
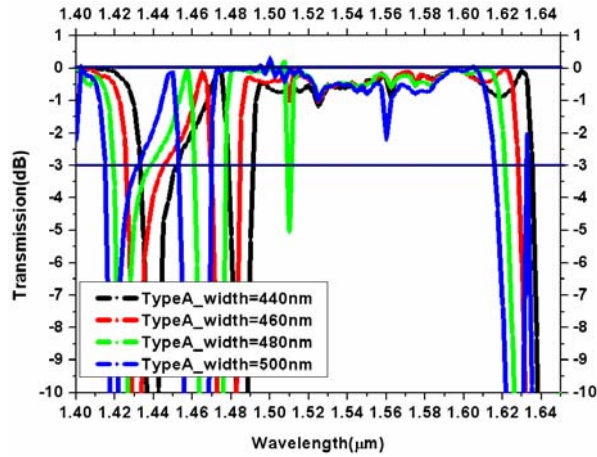
mirrors are 260, 280, 300nm in Type A

Fig 3.25 The width of mirrors are 440, 460, 480, 500 nm in Type A

Table 3   Type A in double 120^0-bend

Mirror width (nm)	High transmission wavelength range (μm)	Transmission bandwidth (nm)
200	1.387μm~1.486μm	99nm
220	1.378μm~1.483μm	105nm
240	1.374μm~1.506μm	132nm
260	1.366μm~1.502μm	136nm
280	1.354μm~1.494μm	140nm
300	1.352μm~1.484μm	132nm
320	1.350μm~1.478μm	128nm
340	1.349μm~1.495μm	146nm
360	1.348μm~1.460μm	112nm
380	1.529μm~1.650μm	136nm
400	1.501μm~1.653μm	152nm
420	1.496μm~1.642μm	146nm
440	1.491μm~1.636μm	145nm
460	1.511μm~1.621μm	110nm
480	1.484μm~1.628μm	142nm
500	1.469μm~1.615μm	146nm

In these figures mention above, when the width of mirrors are 400nm, 420nm, 440nm, 460nm, 500nm, the transmission spectrum have about 150nm broad-band, and the broad band is around 1.55μm. When the mirror of width is 500nm it has 150nm bandwidth and the transmission spectrum is shown in fig. 3.26(s), the TE wave propagation situation is shown in fig. 3.26 (b).
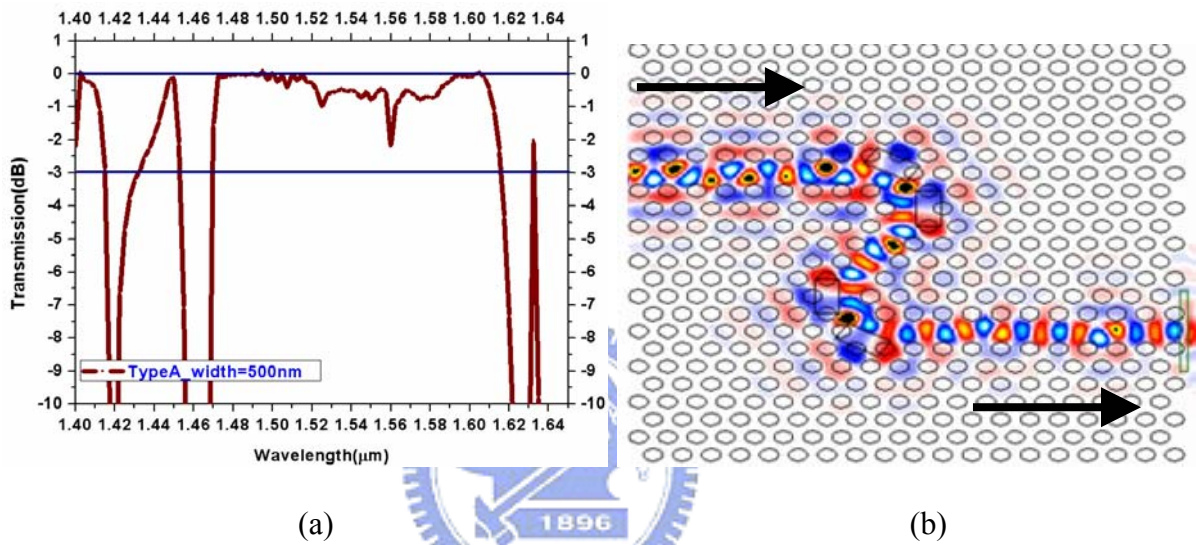

(a)   (b)

Fig. 3.26   (a) The transmission spectrum of the width of mirror is 500nm in Type-A for 120^0-bend photonic crystal waveguide (b) The TE field propagation at wavelength 1.55μm

In type B, four rectangular mirrors are added at 120^0-bend region and to simulate the transmission spectra per 20nm increased from the width of mirror is 180nm. We tune the width of the mirrors along one direction and parallel the channel. The transmission spectra are shown fig. 3.27~ fig. 3.29 and the bandwidth is shown in Table 4, the transmission (dB) is used the formula 10*log(P_{out}/P_{in}). P_{out} is the out put intensity of design waveguide, P_{in} is output intensity of the reference waveguide which is a line defect waveguide. And the high transmission is defined the transmission >-3dB.
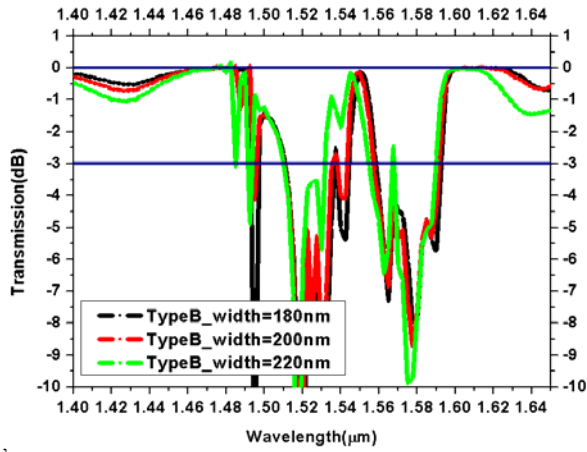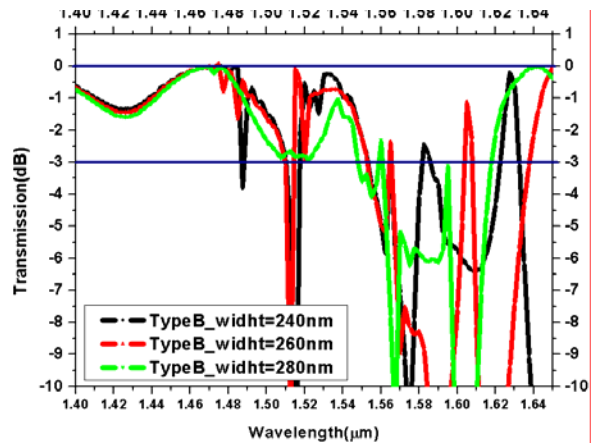
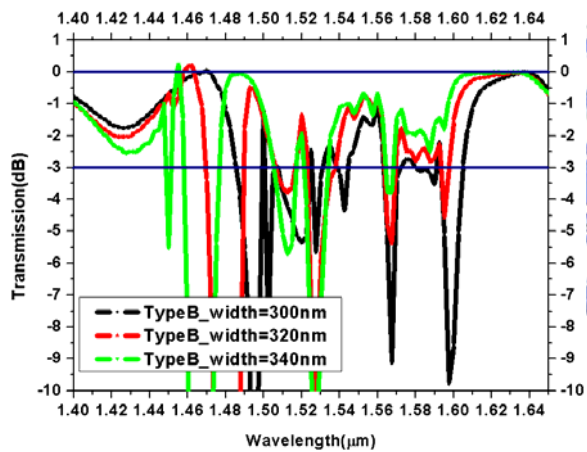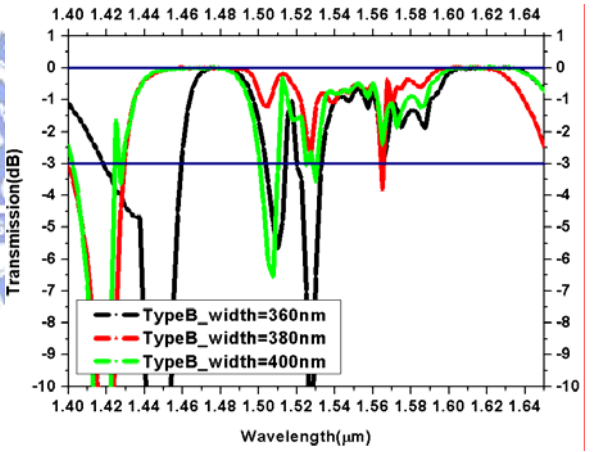(a)   (b)

Fig. 3.27 (a) The width of mirrors are 180nm, 200nm, 220nm in Type-B (b) The width of

mirrors are 240, 260, 280nm in Type B.

(a)   (b)

Fig. 3.28 (a) The width of mirrors are 300, 320, 340nm in Type B (b) The width of mirrors
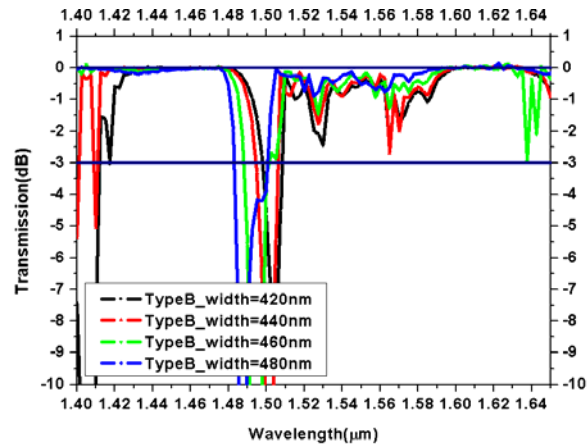
are 360,380,400nm in Type B.

Fig 3.29 The transmission spectrum of mirrors width which are 420, 440, 346, 480nm in

Type B.

Table 4   Type B in double 120^0-bend

Mirror width (nm)	High transmission wavelength range (µm)	Transmission bandwidth (nm)
200	1.360µm~1.493µm	133nm
220	1.355µm~1.484µm	129nm
240	1.354µm~1.486µm	132nm
260	1.354µm~1.508µm	154nm
280	1.353µm~1.525µm	172nm
300	1.352µm~1.484µm	132nm
320	1.352µm~1.470µm	118nm
340	1.568µm~1.671µm	103nm
360	1.533µm~1.668µm	135nm
380	1.430µm~1.565µm	135nm
400	1.531µm~1.664µm	133nm
420	1.508µm~1.661µm	153nm
440	1.506µm~1.651µm	145nm
460	1.501µm~1.637µm	137nm
480	1.500µm~1.668µm	168nm
500	1.495µm~1.651µm	156nm

In fig. 3.30 the bandwidth vs. the width of mirrors in Type A and Type B for double 120^0- bend PCWGs is shown.
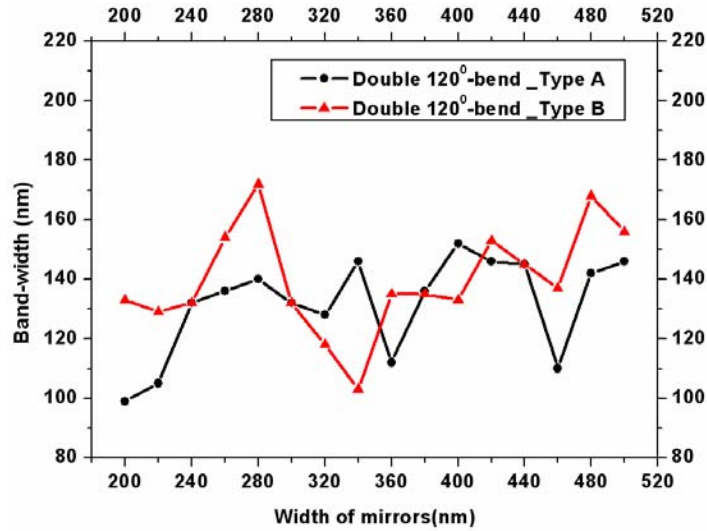

Fig. 3.30 The bandwidth vs. the width of mirrors in Type A and Type B for double 120^0- bend PCWGs

From figures 3.27~3.29, the broad-bend transmission spectra are about 150nm when the width of mirrors are over 420nm. When the width of mirrors is 480nm, the transmission spectrum is from 1.5μm to 1.65μm, it has more potential to enhance the broad-band transmission. When the positions of mirrors are adjusted but the width of mirrors unchanged. In fig 3.31 (a), the mirrors shift toward channel 10, 20, 30, 40nm, then transmission spectrum is shown in fig 3.31 (b). The transmission spectrum has been enhanced by shifting the positions of mirrors, and the broad-band is from 1.392μm ~ 1.634μm around 1.55μm and less than 2dB . The band-width is bigger than 240nm and the TE field propagation is shown in fig. 3.32 and it has about 55 nm no loss from 1.585μm ~1.640μm

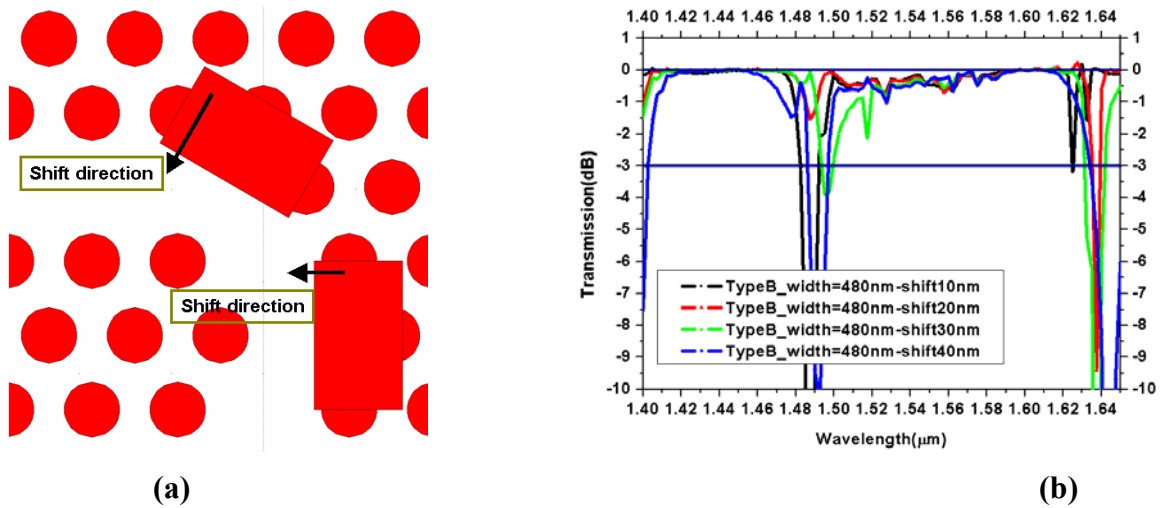|	
(a)	**(b)**

Fig 3.31 (a) It's the direction to shift the mirrors 40nm to the channel of the width of mirrors
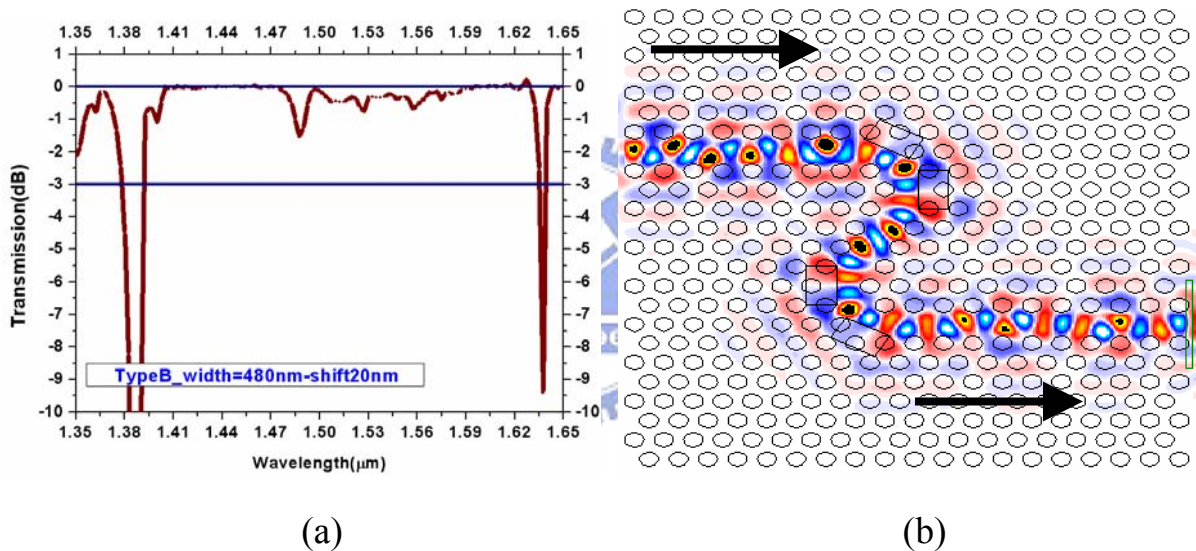are 480nm in type-B, (b) The transmission spectrum versus the shift distance.

(a)	(b)

Fig. 3.32 (a) The transmission spectrum of the width of mirror is 480nm and shitted to
channel 20nm in Type-B (b) The TE field propagation at wavelength 1.55μm.

3.3.3 Summary

In chapter three, designs for broadband transmission double-60°-bend and
double-120°-bend photonic crystal waveguides are investigated using 2D
finite-difference-time-domain method. Planer mirrors are added at the bend region for total
internal reflection and adjust the widths and positions of mirrors for maximum transmission
bandwidth. The transmission result is very sensitive to the widths of the mirrors and the

position of mirrors. Planer mirrors are set at bend-region for double 60^0-bend and 120^0-bend photonic crystal waveguides to get broad-band and high transmission around 1.55μm. There are two ways to add mirrors at the bend region for double 60^0 and double 120^0 bend photonic crystal, one is to dig rectangular mirrors at bend region and increased the width of mirrors uniformly, it's called type-A. Another way is also to add mirrors at bend-region, but increased the width of mirrors parallel the channel, it's called type-B.

For double 60^0 photonic crystal waveguides, when the width of mirrors is 440nm in type-A, it has 189nm band-width, when the width of mirrors is 240nm in type-B it has over 270nm band-width.

For double 120^0 photonic crystal waveguides, t when the width of mirrors is 400nm, 420nm, 440nm, 460nm, 500nm in type-A, it has about 150nm broad-band, when the width of mirrors is 480nm in type-B, it has about 150nm band-width. But the mirrors shift toward channel 20nm, 230nm band-width and high transmission around 1.55μm can be achieved.